Ocean Engineering 220 (2021) 108427

Contents lists available at ScienceDirect

Ocean Engineering

journal homepage: www.elsevier.com/locate/oceaneng

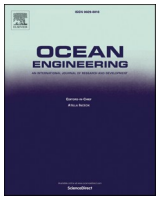

Time-domain analysis of vortex-induced vibration of a flexible mining riser transporting flow with various velocities and densities

Jinlong Duan [a,*], Jifu Zhou [a,b], Yunxiang You [c,d], Xu Wang [a,b]

[a] CAS Key Laboratory for Mechanics in Fluid Solid Coupling Systems, Institute of Mechanics, Beijing, 100190, China
[b] School of Engineering Sciences, University of Chinese Academy of Sciences, Beijing, 100049, China
[c] Collaborative Innovation Center for Advanced Ship and Deep-Sea Exploration, Shanghai Jiao Tong University, Shanghai, 200240, China
[d] State Key Laboratory of Ocean Engineering, Shanghai Jiao Tong University, Shanghai, 200240, China

ARTICLE INFO

Keywords:
Vortex-induced vibration
Internal flow
Time domain prediction method
Coupling of in-line and cross-flow responses

ABSTRACT

Vortex-induced vibration (VIV) can be inevitably encountered in deep ocean mining. As the internal flow is transported axially in the flexible riser, complicated VIV dynamics occurs undergoing both the internal and external flows. Therefore, the object here is to explore the effect of the internal flow with different velocities and densities on VIV response under various uniform current. In this study, a semi-empirical time domain prediction method for VIV dynamics of flexible risers considering both internal and external flows is introduced and adopted. The governing equations are discretized and solved by using finite element method. Firstly, validations are made for VIV without internal flow based on the numerical results and experimental data. Comparisons prove that the simulation could reproduce the VIV dynamics of a flexible riser. Then with the increase of the internal flow velocities and densities, the effect of the internal flow on VIV response is examined. It is found that the dominating frequency and the root mean square (RMS) displacement in both in-line (IL) and cross-flow (CF) directions are notably influenced by the internal flow velocity and density. Besides, the drag coefficient and IL mean deflection are detected magnified while the internal flow velocity and density are increased under different external flow velocities. It should be noted that the change of the internal flow velocity and density could trigger new mode response of the flexible riser, leading to mode transition for the IL and CF dominating modes. In addition, VIV dynamics shows a similar changing trend with the increase of the internal flow velocity and density when the flexible fluid-conveying riser is subjected to different external flow velocities.

1. Introduction

As the traditional land-based mines might hardly meet the demands for global development in the future, much attention has been paid to deep sea mining because of its abundant mineral deposits (Ali et al. (2017); Sharma (2017)). Although great efforts have been made to develop the technology of deep sea mining for decades, many challenges still exist in the progression of commercializing deep sea mining. As a critical component, flexible risers are inevitably subject to currents and waves while transporting oil, gas or mineral ores from seabed to platforms. As a consequence, vortex-induced vibration (VIV) occurs due to the periodical hydrodynamic forces exerting on the transporting risers for such an ocean mining system. And VIV is particularly crucial for flexible risers. Since the ocean resource exploration has further moved to deep waters recently, the risers become much slenderer, which can lead to complicated VIV dynamics under different environmental factors. For decades, engrossing works have been carried out to investigate VIV response of rigid and flexible risers experimentally and numerically, as seen in the comprehensive reviews of Sarpkaya (2004), Williamson and Govardhan (2008) and Bearman (2011).

Since flexible risers are extensively used in ocean engineering, the VIV response of such risers has drawn much attention. Recently, flexible risers with different aspect ratios have been studied by many researchers (Vandiver (1993a,b); Seyed-Aghazadeh et al. (2019); Chaplin and King (2018); Xu et al. (2018); Song et al. (2011)). Some common characteristics of VIV, such as multiple modes vibration and traveling wave response, are observed during their researches. Furthermore, experimental studies have been performed to investigate the VIV dynamics of flexible risers under uniform and sheared currents (Trim et al. (2005); Huera-Huarte et al. (2014); Gao et al. (2015)). And VIV response of

* Corresponding author.
E-mail address: duanjl@imech.ac.cn (J. Duan).

https://doi.org/10.1016/j.oceaneng.2020.108427
Received 2 July 2020; Received in revised form 22 September 2020; Accepted 26 November 2020
Available online 9 December 2020

risers subjected to uniform and sheared currents has also been studied based on various methods of numerical simulation (Violette et al. (2010); Wang and Xiao (2016); Joshi and Jaiman (2017); Joshi et al. (2017); Qu and Metrikine (2020)). These researches help us to have a thorough understanding of VIV mechanism and dynamics on flexible risers. And the VIV response of flexible risers has been proved more complicated while the sheared current is considered. Although VIV dynamics has been comprehensively analyzed in these works, the VIV response of flexible risers is studied only with the consideration of external flow. Nevertheless, the underlying VIV mechanism and dynamics of flexible risers with the combination of internal and external flows are still much less understood. As the flexible risers are responsible for conveying oil and gas or mineral ores from seabed to platforms in ocean industry, the effect of internal flow on the VIV dynamics cannot be ignored under this circumstance.

Therefore, the investigation on the internal flow effect on risers is of great significance and interest, especially with the increase of the aspect ratio of risers in ocean mining system (Atadan et al. (1997); Chatjigeorgiou (2010)). Since internal force exerting on the pipe inside (e.g., centrifugal and Coriolis accelerations) can be induced while the flexible riser conveys fluid, experiments and simulations have been carried out to examine the effect of internal flow on the riser vibration. Without considering the external flow, the dynamics of a fluid-conveying pipe has been researched by Païdoussis (2014). It is observed that the pipe may lose stability at some critical values of the internal flow velocity. Moreover, experimental and numerical studies can be found for the investigations on the effect of the internal flow recently (Ortega et al. (2012); Cabrera-Miranda and Paik (2019); Zhu et al. (2018)). These researchers mostly focus on the interaction between the flexible riser vibration and internal slug flow. Apart from these studies, the effect of the internal flow on the VIV dynamics has been studied by Guo and Lou (2008), Meng et al. (2017), Yang et al. (2018), Jiang et al. (2019), Wang et al. (2018) and Duan et al. (2018). While both the internal and external flows are taken into account, some VIV characteristics are found more complicated due to fluid structure interaction, such as lock-in response, vibrating trajectory and quasi-periodic oscillation. Besides, the CF VIV of pipes or steel catenary risers conveying fluid in the subcritical or supercritical regimes are examined (Keber and Wiercigroch (2008); Meng and Chen (2012); Dai et al. (2013)), which proves the effect of internal flow cannot be ignored.

Although the VIV dynamics of risers considering both internal and external flow has become an engrossing issue and drawn much attention, there are few published literatures reporting the VIV response of ocean mining risers with various densities. Since the risers for deep sea mining transports mineral ores, the internal flow density is higher, which may cause that the VIV dynamics of slender risers can be influenced by the internal flow significantly. Recently, the topic has been paid attention by some researchers (Knudsen et al. (2016); Thorsen and Sævik (2018); Thorsen et al. (2019)). During their studies, the effect of the internal flow density on the curvature and fatigue damage of the riser is studied and analyzed. Although there exist a few studies of VIV dynamics of risers with internal and external flows, it is not enough to have a thorough understanding of VIV mechanism and dynamics of flexible risers with the consideration of internal and external flows, quantitatively and qualitatively, especially for the flexible risers with various internal flow velocities and densities. Therefore, based on the pure internal flow theory and the semi-empirical hydrodynamic model, this study is motivated to investigate the effect of internal flow on the three-dimensional VIV response of a flexible riser with the change of the internal flow velocity and density.

During the simulation, a semi-empirical time domain prediction method developed by Zhang et al. (2018) is presented and adopted. In Section 2, the three-dimensional model of a flexible riser with internal flow and the hydrodynamic model applied for a flexible riser are elaborated. Then, comparison is made to verify the feasibility and reliability of our simulation in Section 3. In addition, the IL and CF VIV dynamics of a flexible riser subject to uniform current with the increase of internal flow velocity and density is examined in this section. In Section 4, conclusion is drawn based on this study and future works are also suggested.

2. Numerical models and solution

2.1. Flexible riser model

The simply supported flexible riser subjected to a uniform current while transporting fluid inside is illustrated in Fig. 1. In this model, the effect of both internal and external flow is taken into consideration. It consists of a flexible riser of length L with mass per unit length m_r, density ρ_r, bending stiffness EI, as well as the internal and external diameters of the riser d_i and D_e respectively. The internal fluid with density ρ_i has a mass of m_f per unit length of the riser and a velocity U_i. The external flow with density ρ_e has a mass of m_e per unit length of the riser. The external imposed tension is assumed to be T, as shown in Fig. 1. Hence, according to Païdoussis (2014), the governing equations of the flexible riser considering both internal and external flows can be represented as:

$$\left(m_r+m_f\right)\ddot{x}+c\dot{x}+2m_fU_i\dot{x}'+\left(m_fU_i^2-T\right)x''+EIx''''=F_{IL} \tag{1}$$

$$\left(m_r+m_f\right)\ddot{y}+c\dot{y}+2m_fU_i\dot{y}'+\left(m_fU_i^2-T\right)y''+EIy''''=F_{CF} \tag{2}$$

Where x and y are the dimensional displacements in IL and CF directions. c represents the structure damping. F_{IL} and F_{CF} are the hydrodynamic forces caused by the external flow in IL and CF directions, including the inertia force, the drag force in IL direction and the vortex-induced force in CF and IL directions.

2.2. Hydrodynamic force model

The hydrodynamic force in this prediction model contains the inertia force, the drag force in IL direction and the vortex-induced force in CF and IL directions (Zhang et al. (2018)). In IL direction, apart from the inertia force, the hydrodynamic force F_{IL} can be decomposed into a drag force F_D and a vortex-induced force $F_{vor,\ IL}$ as

$$F_{IL}=-m_a\ddot{x}+F_D+F_{vor,\ IL} \tag{3}$$

where the added mass $m_a=C_am_e$ with added mass coefficient $C_a=1.0$. While the hydrodynamic force F_{CF} can be decomposed into a vortex-induced force $F_{vor,\ CF}$ and the inertia force with the same added mass as

$$F_{CF}=-m_a\ddot{y}+F_{vor,\ CF} \tag{4}$$

2.2.1. Drag force model

During the simulation, the drag force F_D in IL direction is calculated based on Morison equation, in which the relative velocities of the external flow and the flexible riser motion are taken into account. The equation is expressed as follows:

$$F_D=\frac{1}{2}\rho_eD_eC_D(U_e-\dot{x})|U_e-\dot{x}| \tag{5}$$

where C_D is the drag coefficient of the cross section along the flexible riser. It should be noted that C_D is not constant at different node z. Here, the prediction model for the drag coefficient of a flexible riser developed by Vandiver (1983a,b) is used.

$$C_D(z)=C_{D0}\left[1+1.043\left(\frac{2y_{RMS}(z)}{D_e}\right)^{0.65}\right] \tag{6}$$

where C_{D0} represents the drag coefficient for a stationary cylinder. And the value of C_{D0} is 1.2 in the subcritical Re regime. $y_{RMS}(z)$ is the RMS of the CF VIV displacement at node z.

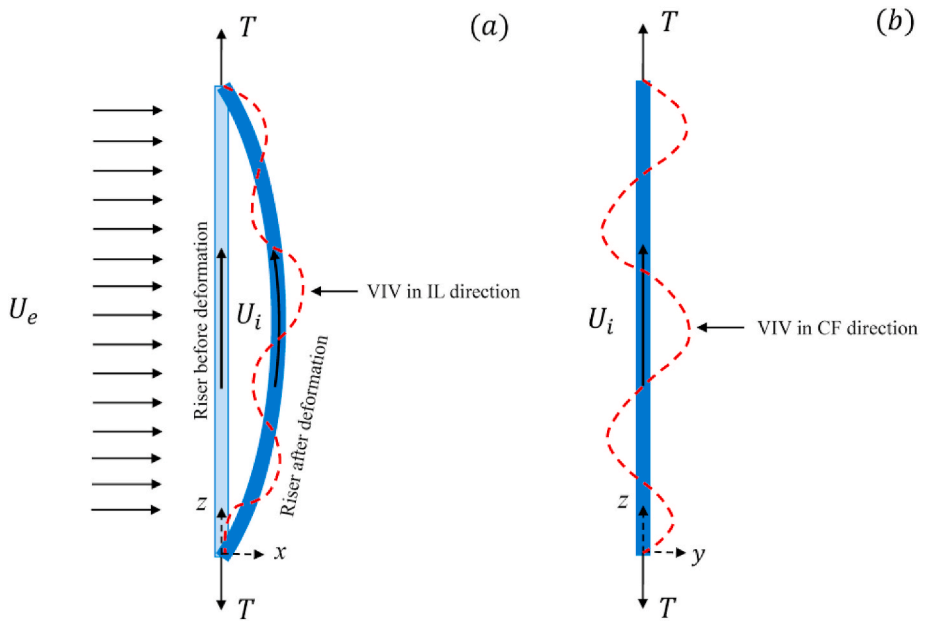

Fig. 1. Sketch of a fluid-conveying riser subjected to uniform current and its VIV responses.

2.2.2. Vortex-induced force model

As mentioned in the former subsection, the hydrodynamic force exerting on the flexible riser includes the vortex-induced forces in IL and CF directions. Such hydrodynamic force can be divided into the excitation force under all excitation frequencies in the exciting region in both CF and IL directions and the hydrodynamic damping force in the damping region in CF direction, as shown in Fig. 2. Hence, it is necessary to identify the flexible riser's exciting and damping regions before the vortex-induced force is exerted.

2.2.2.1. Determination of excitation and damping regions. Based on the conventional empirical model methods, the excitation and damping regions of the flexible riser are determined (Passano et al. (2016)). Firstly, the non-dimensional frequency of the flexible riser is required to be identified according to the following equations:

$$f^*_{IL,i} = \frac{\omega_{IL,i}}{2\pi}\frac{D_e}{U_e} \tag{7}$$

$$f^*_{CF,j} = \frac{\omega_{CF,j}}{2\pi}\frac{D_e}{U_e} \tag{8}$$

where $\omega_{IL,i}$ and $\omega_{CF,j}$ are the i^{th}- and j^{th}-order natural frequencies of the flexible riser in IL and CF directions.

Note that the Strouhal number obtained based on an experiment of a rigid cylinder is $St = 0.19$. As the Reynolds number is not constant during the simulation, $St = 0.19$ is not always suitable here, as shown in

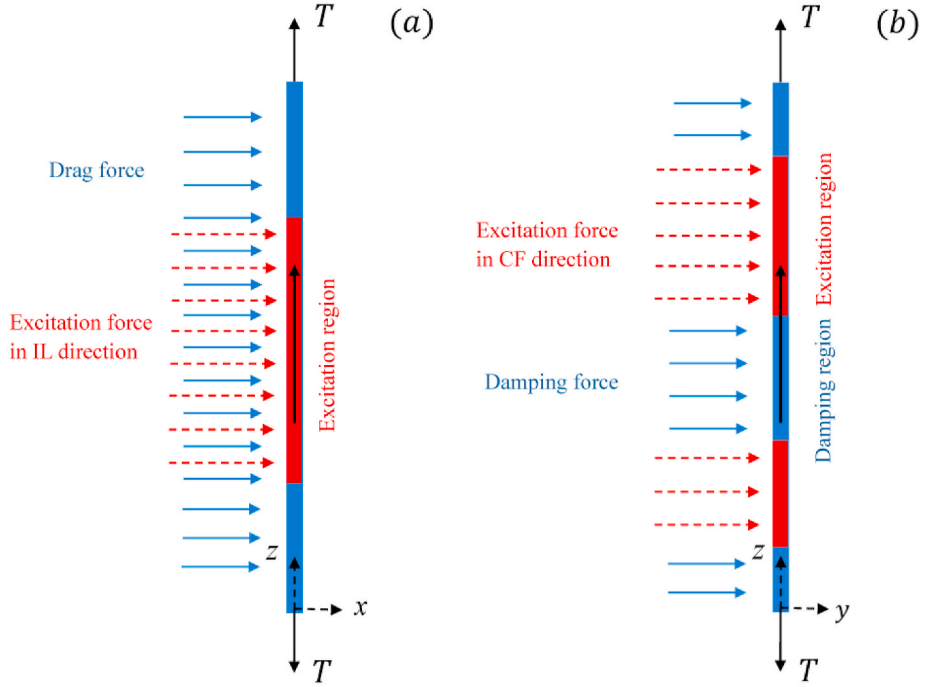

Fig. 2. Hydrodynamic forces on excitation and damping regions of a flexible riser.

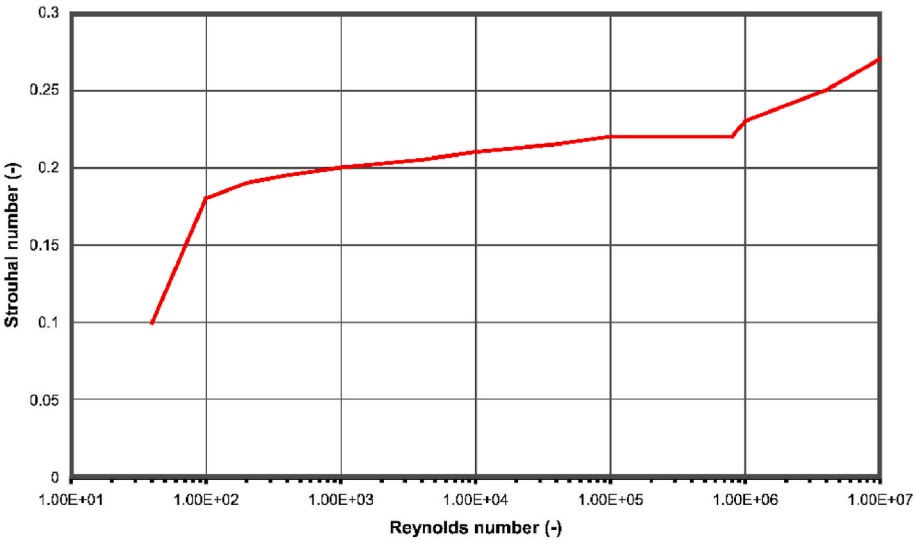

Fig. 3. Strouhal number as function of Reynolds number (Passano et al. (2016)).

Fig. 3 (Passano et al. (2016))). Therefore, the non-dimensional frequency needs to be modified based on the real Reynolds number of the fluid. And it is modified by the following equation:

$$f^*_{Gij} = \frac{St \cdot f^*_{ij}}{St^*} \tag{9}$$

where $St = 0.19$ and St^* is the Strouhal number calculated based on the real Reynolds number according to Fig. 3.

After the modification of the natural frequency, the excitation and damping regions of the flexible riser can be identified based on the criteria below, as shown in Eqs. (10) and (11).

$$0.25 \leq f^*_{Gi,\ IL} \leq 0.6 \tag{10}$$

$$0.125 \leq f^*_{Gj,\ CF} \leq 0.2 \tag{11}$$

The excitation regions in IL and CF directions are defined whether the non-dimensional IL and CF natural frequency of the flexible riser at node z satisfies Eqs. (10) and (11), respectively. If so, node z of the flexible riser will be located in the excitation region of the i^{th} and j^{th} excitation frequencies in IL and CF directions respectively, as illustrated in Fig. 4. Otherwise, it will be located in the damping region.

It should be emphasized that plenty of works have proved that the VIV response is almost always dominated by one frequency even if there are many response frequency candidates (Lie et al. (1997)). In other words, the dominating frequency could take its total excitation region, while other frequencies will take their own regions from segments along the flexible riser that have not been taken by frequencies with higher priority. Correspondingly, there is one excitation frequency in a certain excitation region of the flexible riser. Therefore, excitation regions of different excitation frequencies do not overlap. But according to Eqs. (10) and (11), there may exist overlapped excitation regions for the multi-frequency response, as shown in Fig. 4. During the simulation, the overlapped region is dealt with based on the assumption of simultaneously acting frequencies in VIVANA (Passano et al. (2016)). In order to define how the excitation regions of the flexible riser should be dominated, the priority of these response frequencies is ranked according to an excitation parameter based on energy considerations (Passano et al. (2016)):

$$E_i = \int U_e^3 D_e^2 \left(\frac{A}{D_e}\right)_{C_L=0} dL \tag{12}$$

where $\left(\frac{A}{D_e}\right)_{C_L=0}$ is the non-dimensional amplitude where the excitation

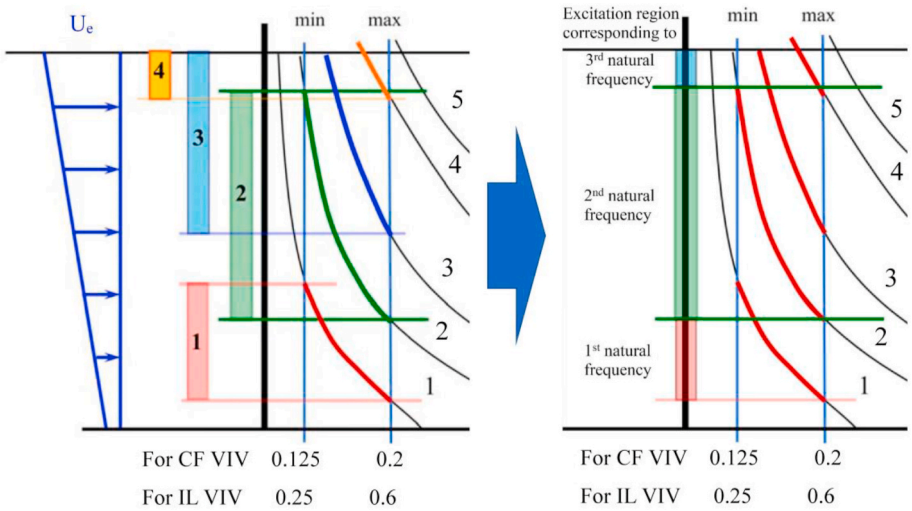

Fig. 4. Excitation regions of the riser corresponding to simultaneous response frequencies (Passano et al. (2016)).

coefficient shifts from positive value to negative one. According to Eq. (12), the priority of the response frequencies can be ranked. The frequency with the largest excitation parameter is referred to as "the dominating response frequency", as demonstrated in Fig. 4.

2.2.2.2. Excitation force model. After the excitation regions are determined, the excitation forces are required to exert on these regions. In this study, the excitation force model due to vortex shedding developed by Sarpkaya (1977) is used to calculate the dynamic excited forces here. The IL and CF excitation forces are expressed as:

$$F_{ex,IL} = \sum_{i=mIL}^{nIL} F_{ex,IL,i} = \sum_{i=mIL}^{nIL} \frac{1}{2}\rho_e D_e U_e^2 C_{L,IL,i}\left[\frac{A_{IL,i}}{D_e}, f^*_{IL,i}\right]\cos\left(\omega_{IL,i}\cdot t + \phi_{IL,i}\right) \quad (13)$$

$$F_{ex,CF} = \sum_{j=mCF}^{nCF} F_{ex,CF,j} = \sum_{j=mCF}^{nCF} \frac{1}{2}\rho_e D_e U_e^2 C_{L,CF,j}\left[\frac{A_{CF,j}}{D_e}, f^*_{CF,j}\right]\cos\left(\omega_{CF,j}\cdot t + \phi_{CF,j}\right) \quad (14)$$

where $C_{L,IL,i}\left[\frac{A_{IL,i}}{D_e}, f^*_{IL,i}\right]$ and $C_{L,CF,j}\left[\frac{A_{CF,j}}{D_e}, f^*_{CF,j}\right]$ are the excitation force coefficients in the excitation region of the i^{th}- and j^{th}-order excitation frequencies in IL and CF directions. And lock-in phenomenon is assumed to occur in the excitation region in order to achieve synchronization. Therefore, the IL and CF excitation force frequencies are supposed to be locked to the i^{th}- and j^{th}-order natural frequencies, respectively. Consequently, the phase difference between the velocity and force will always be the initial phase angle of the force, since ratio of the force frequency and velocity frequency is 1.0. Note that the initial phase angles $\phi_{IL,i}$ and $\phi_{CF,j}$ are related to the excited modes in IL and CF directions. The values of $\phi_{IL,i}$ and $\phi_{CF,j}$ can be set to be 0 and π according to the excited mode shape. As shown in Fig. 5, $\phi_{IL,i} = 0$ and $\phi_{CF,j} = 0$ are adopted while the value of excited mode shape at riser nodes is positive. Otherwise, $\phi_{IL,i} = \pi$ and $\phi_{CF,j} = \pi$. As a consequence, the IL and CF excitation force frequencies will catch up with the i^{th}- and j^{th}-order natural frequencies in IL and CF directions, respectively.

The IL and CF excitation force coefficients $C_{L,IL,i}$ and $C_{L,CF,j}$ are obtained based on a strip theory. It should be noted that hydrodynamic coupling along the flexible riser is not considered and the coupling effects are only considered by the structure. In addition, the effect of Reynolds number on excitation coefficients are not taken into account here according to Zhang et al. (2018). The values of $C_{L,IL,i}$ and $C_{L,CF,j}$ can be calculated based on the database in VIVANA (Passano et al. (2016)). The IL and CF excitation coefficients corresponding to IL and CF nondimensional vibration amplitude under a non-dimensional frequency can be obtained according to the data illustrated in Figs. 6 and 7. After the IL and CF excitation coefficients are obtained from the database, the instantaneous excitation coefficients in IL and CF directions can be calculated based on the curve fitted in Fig. 8. And the IL and CF excitation coefficients will be updated at each moment according to the excitation frequency at this moment. As a result, the IL and CF excitation coefficients will be constant over the periods of stable oscillation. It should be emphasized that the effects of Reynolds number on excitation coefficients are not taken into consideration during our simulation. In the initial calculation step, the maximum excitation coefficients for IL and CF responses are adopted in order to excite the VIV response.

2.2.2.3. Hydrodynamic damping force model. During the simulation, the hydrodynamic damping force in CF direction proposed by Thorsen et al. (2014) is adopted. The equation is as follows:

$$F_{damp,CF} = -\frac{1}{2}\rho_e D_e C_1 U_e \dot{y} - \frac{1}{2}\rho_e A_y C_2 \dot{y}|\dot{y}| \quad (15)$$

where $F_{damp,CF}$ is the CF hydrodynamic damping force in the damping region. A_y is the CF amplitude of the flexible riser. C_1 and C_2 are empirical coefficients, both of which are equal to 0.485 and 0.936, respectively (Thorsen et al. (2014)).

2.3. Solution method

Firstly, the governing equations of the flexible riser with both internal and external flows are discretized and solved by finite element method and Newmark-β method. The differential equation of motion for the riser can thus be expressed as

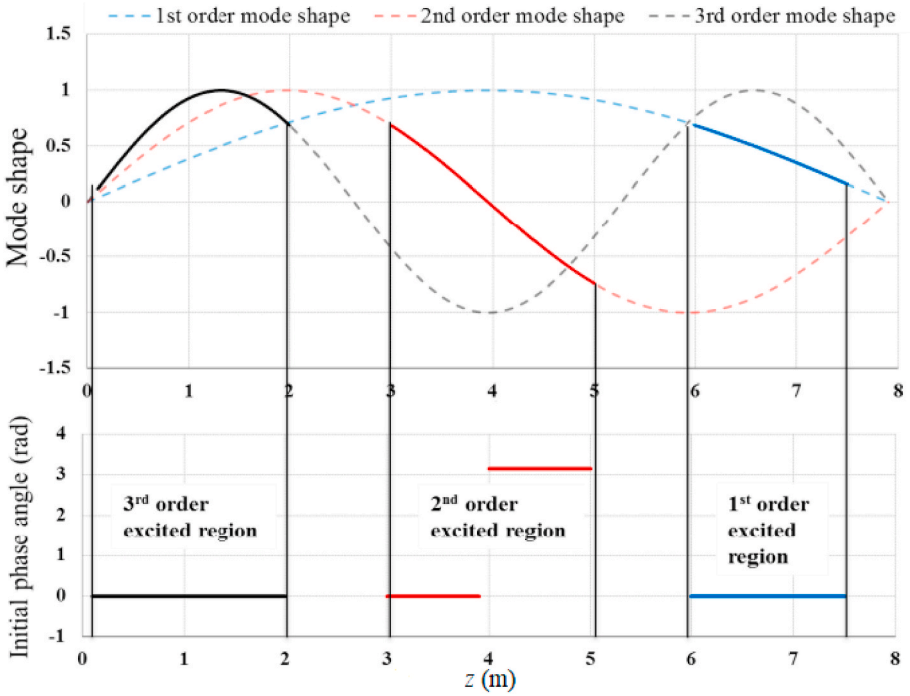

Fig. 5. The initial phase angles for VIV response (Zhang et al. (2018)).

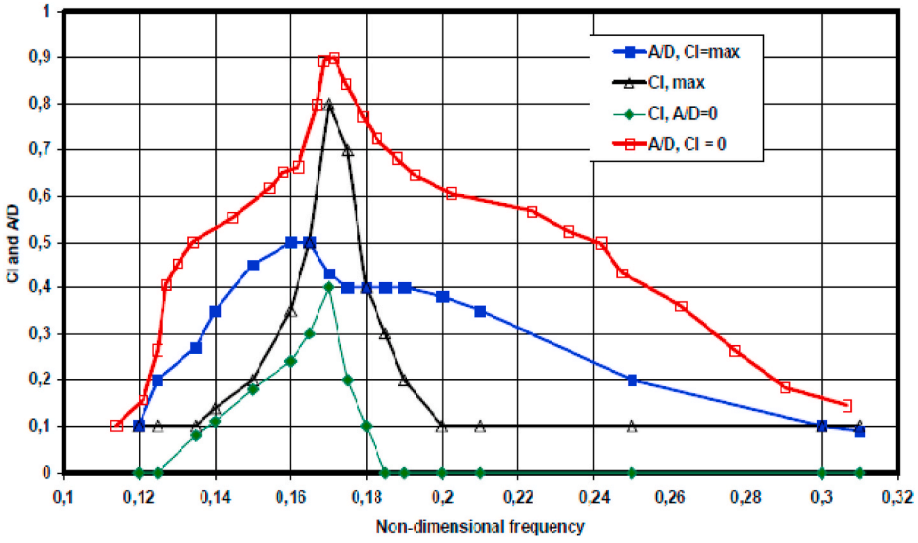

Fig. 6. CF Excitation coefficient model (Passano et al. (2016)).

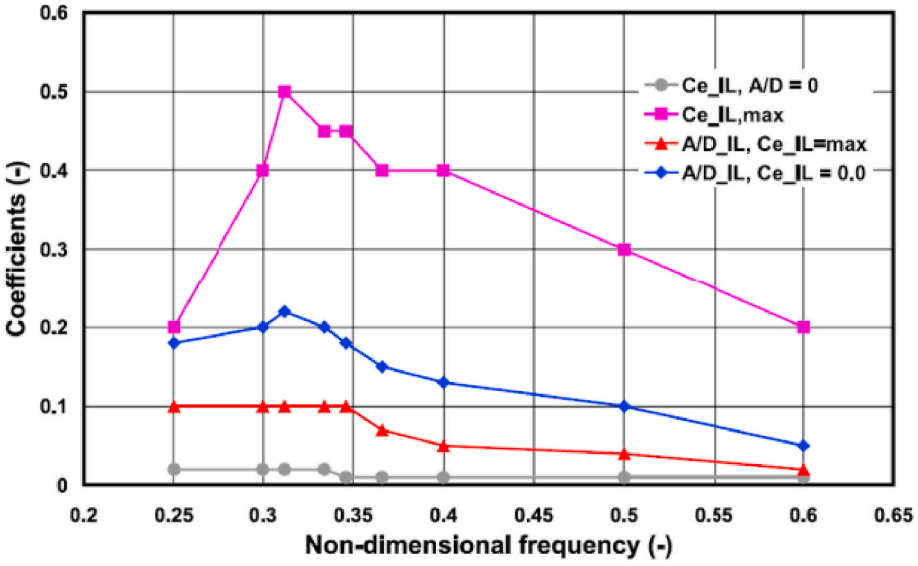

Fig. 7. IL Excitation coefficient model (Passano et al. (2016)).

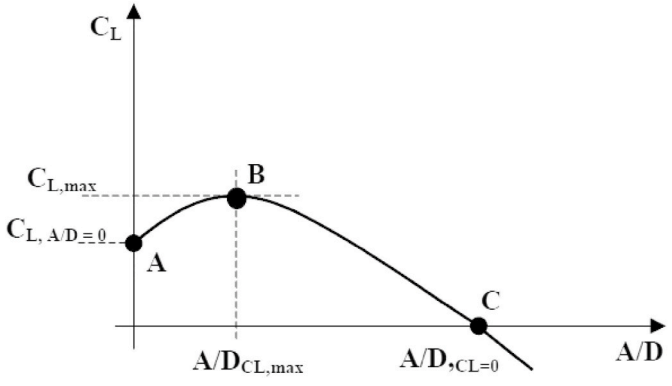

Fig. 8. Function of the excitation coefficient vs nondimensional amplitude (Vandiver (2003)).

$$\mathbf{M}\ddot{d}(t) + \mathbf{C}\dot{d}(t) + \mathbf{K}d(t) = \mathbf{F}(t)$$

where **M, C** and **K** are the mass matrix, damping matrix and stiffness matrix of the riser, respectively. The Rayleigh damping model is applied to calculate the damping matrix **C**. And the parameters of Rayleigh damping model are obtained based on the first and second dominant mode frequencies. The Newmark-β method with $\beta = 0.25$ and $\gamma = 0.5$ is applied. Then the dynamic response of the riser considering internal flow is examined in time domain. The detailed calculation procedures can refer to those expressed by Zhang et al. (2018) and will not be elaborated here.

3. Results and discussion

In this section, the present model is firstly verified by comparison with experimental data in order to prove the validity and accuracy of this method. Then the three-dimensional VIV dynamics of the flexible riser with various internal flow velocities and densities is investigated and analyzed.

3.1. Validation of simulation

For the VIV validation of a flexible riser, the experiment carried out by Song (2016) is introduced here. And the parameters of the flexible riser model are listed in Table 1. Then, the dynamic responses of the riser without internal flow are simulated in time domain.

3.1.1. Examination of element number and time step dependency

Firstly, the dependency of the model on the element number and time step is examined based on the numerical results and experimental data. With different element numbers and time steps, the percentage errors of the maximum value of IL and CF RMS displacements are calculated and presented in Table 2 and Table 3.

It can be seen that while the element number N is 50, the percentage errors of $[x/D_e]^{max}_{RMS}$ and $[y/D_e]^{max}_{RMS}$ are relatively high during our calculation, especially for the CF VIV response with an error over 10%. However, the percentage errors of $[x/D_e]^{max}_{RMS}$ and $[y/D_e]^{max}_{RMS}$ are evidently decreased when the riser model is divided into 100 and 200 elements. All the percentage errors with $N = 100$ and 200 are less than 10% (Table 2). Hence, it can be concluded that the percentage error in the results predicted with $N = 100$ and 200 is within the acceptable range.

Likewise, the convergence can also be confirmed by decreasing the time step Δt while $N = 100$, as shown in Table 3 and Fig. 9. It can be observed that the amplitudes in IL direction is underestimated when $\Delta t = 0.002$s compared with the numerical results under other time steps (Fig. 9). In addition, the percentage error of $[x/D_e]^{max}_{RMS}$ is up to 25.79% with $\Delta t = 0.002$s here, as presented in Table 3. But when the time step $\Delta t = 0.001$s, 0.0005s and 0.0002s, the IL and CF displacements are almost the same and the percentage errors of $[x/D_e]^{max}_{RMS}$ and $[y/D_e]^{max}_{RMS}$ are less than 10%. Therefore, based on the discussions above and also taking into account the computational efficiency, the investigations during our simulation are conducted with element number $N = 100$ and time step $\Delta t = 0.001$s. Correspondingly, the flexible riser model is divided into 100 finite elements, as illustrated in Fig. 10.

3.1.2. Validation based on experimental data

The predicted IL and CF RMS displacements and the amplitude spectrum of the flexible riser's midpoint under uniform current $U_e = 1.6$m/s are shown in Fig. 11 and Fig. 12, respectively. Note that the IL and CF RMS displacements and IL mean deflection are non-dimensionalized with the outer diameter of the riser D_e in our study.

It can be seen from Fig. 11 that the predicted dominating frequencies of the flexible riser's midpoint are 19.05 Hz and 8.8 Hz in IL and CF directions respectively, which are close to the experiment results 18.15 Hz and 9.08 Hz (Song (2016)). And the IL and CF RMS displacements show a good agreement with the experiment data, as shown in Fig. 12. Note that although the IL and CF RMS displacement is slightly overestimated compared with the experimental results, the right dominant modes and frequencies of VIV in IL and CF directions can be predicted by this method. But there exists reasonable discrepancy for the RMS displacements in IL and CF direction, which can also be found in Song (2016). The discrepancy of the IL and CF RMS displacements can be attributed to that the excitation coefficients are obtained based on the purely CF forced oscillation tests of rigid cylinder by Gopalkrishnan (1993) and the combined IL and CF forced oscillation of rigid cylinder by Soni (2008). In the present simulation, a flexible riser is studied. For the lack of excitation coefficient database from available experimental results of flexible risers, the excitation coefficients obtained from rigid cylinders are utilized here. Another potential factor for the discrepancy is that the values of added mass coefficients are set as 1.0. There are researches finding that the added mass coefficients of flexible risers have significant difference with those of rigid cylinders and can take various values within the lock-in region (Song et al. (2016); Bourguet et al. (2011)). Although some discrepancies are observed which is expected as the excitation coefficients are from experiments of rigid cylinders and the added mass coefficient is assumed to be a constant for simplicity, it can be concluded the time domain simulation model is capable of reproducing important quantities of VIV such as the IL and CF dominant modes and frequencies, as well as the RMS displacements in both IL and CF directions, based on the caparison with the experimental data.

Table 1
Parameters of the flexible riser model (Song (2016)).

Parameter	Value
Length L (m)	7.9
Bending stiffness EI (N· m^2)	1476.76
Outer diameter D_e (m)	0.031
Inner diameter d_i (m)	0.027
Pretension T (N)	3000
Mass per unit m_r (kg)	1.768
Damping ratio c (%)	0.3

Table 2
The percentage errors with different element numbers.

Element number	RMS displacement			
	$[x/D_e]^{max}_{RMS}$	Error (%)	$[y/D_e]^{max}_{RMS}$	Error (%)
$N = 50$	0.1601	−1.66	0.4254	−12.14
$N = 100$	0.1645	1.04	0.5079	4.89
$N = 200$	0.1634	0.37	0.5053	4.36
Experiment (Song (2016))	0.1628	–	0.4842	–

Table 3
The percentage errors with different time steps.

Time step	RMS displacement			
	$[x/D_e]^{max}_{RMS}$	Error (%)	$[y/D_e]^{max}_{RMS}$	Error (%)
$\Delta t = 0.002$s	0.1208	−25.79	0.5081	4.93
$\Delta t = 0.001$s	0.1645	1.04	0.5079	4.89
$\Delta t = 0.0005$s	0.1639	0.68	0.5063	4.56
$\Delta t = 0.0002$s	0.1637	0.55	0.5045	4.19
Experiment (Song (2016))	0.1628	–	0.4842	–

3.2. VIV dynamics of a flexible riser with different internal flow velocities

For the flexible riser studied here, the variation of the dimensional natural frequencies with the increase of the internal flow velocity is illustrated in Fig. 13. It can be seen that with the increase of the internal flow velocity, all the natural frequencies decrease, which has the same varying trend with former studies of Païdoussis (2014) and Dai et al. (2013). During our simulation, the three-dimensional VIV dynamics of a flexible riser subjected to uniform current $U_e = 1.6$m/s is investigated by increasing the internal flow velocity, based on the empirical predicted model elaborated in the previous section. And the VIV displacements, dominating modes and frequencies in IL and CF directions are mainly analyzed with the internal flow density equal to 2000 kg/m^3 ($\rho_i = 2000$kg/m^3).

3.2.1. IL and CF RMS displacements and dominating modes

Firstly, the effect of the internal flow velocity on the CF and IL RMS displacements of the flexible riser is examined. As seen in Figs. 14 and 15, when the external flow velocity $U_e = 1.6$m/s and the internal flow density $\rho_i = 2000$kg/m^3, the 4th and 5th mode responses of the flexible riser are excited in IL and CF directions without internal flow velocity ($U_i = 0$m/s), respectively.

When the internal flow velocity is taken into account, the maximum CF RMS displacements increase with the increase of U_i. It can be seen that the maximum CF RMS displacement is around $[y/D_e]_{RMS} = 0.5$ with

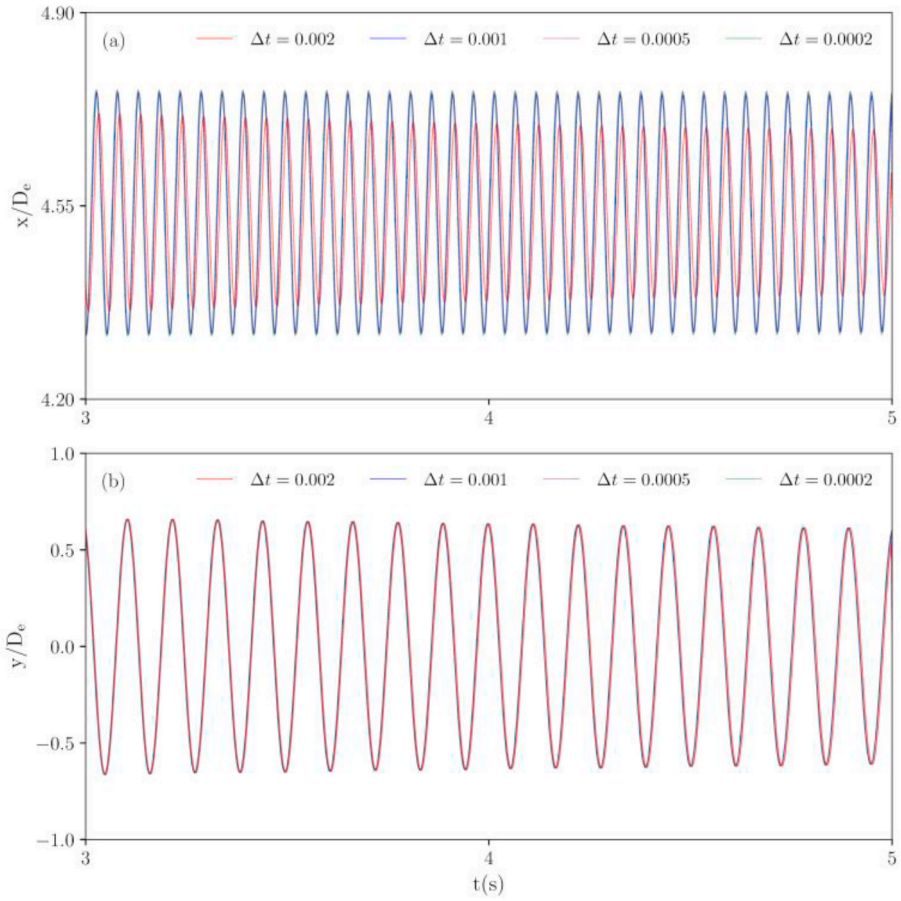

Fig. 9. Time histories of IL and CF vibration with different time steps Δt.
(a) The IL vibration; (b) The CF vibration.

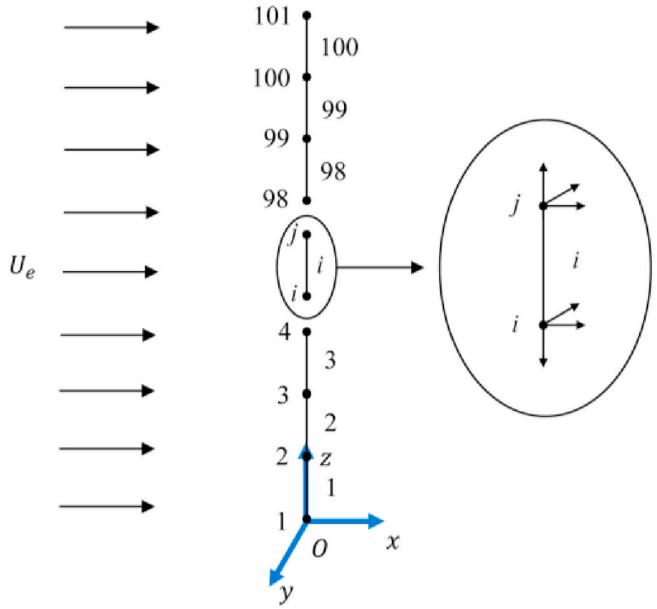

Fig. 10. Finite element model of the flexible riser.

$U_i = 0$m/s. When the internal flow velocity is increased, the maximum value of CF displacement begins to magnify. And the value of $[y/D_e]_{RMS}$ can reach up to approximately 0.65 while $U_i = 40$m/s. This variation can be attributed to the influence of the internal flow. As the internal flow is taken into consideration, more power flows into the structural system, causing the CF RMS displacements to grow. When the energy into the flexible riser balances the energy out of the structure, the oscillations of the flexible riser are regular and repeatable with larger amplitudes (Fig. 14). With the increase of the internal flow velocity, more power flows into the flexible riser system, which leads to the riser vibration with larger peak RMS displacements in CF direction, as shown in Fig. 14.

After removing the mean deflection from the overall IL displacements, the RMS displacement of the flexible riser in IL direction $[x/D_e]_{RMS}$ is plotted in Fig. 15. It is evident that the maximum value of the IL RMS displacement is approximately 0.14 for $U_e = 1.6$m/s and $U_i = 0$m/s. When the internal flow velocity is increased, the maximum IL RMS displacements decrease under the same external flow velocity. But the decreases are not very notable when the change of internal flow velocity is not large enough, as shown in Fig. 16. While U_i is increased dramatically, the decrease of the maximum IL RMS displacement can be observed evidently. For example, the maximum values of the IL RMS displacement can be reduced to approximately 0.135 and 0.115 respectively when $U_i = 20$m/s and $U_i = 40$m/s in our study. The reason for such decrease is that the increase of the IL mean deflection can be contributed to the decrease of the IL RMS displacement. With larger IL mean deflection, the flexible riser vibrates with small amplitudes in IL direction. Moreover, another potential factor is that the change of the power transferred into the riser system can also account for the decrease of IL RMS displacement. Although more power is transferred into the riser system compared with the riser system without internal flow, the percentage of the power responsible for the increase of the IL mean deflection and CF RMS displacement is relatively high, causing that less

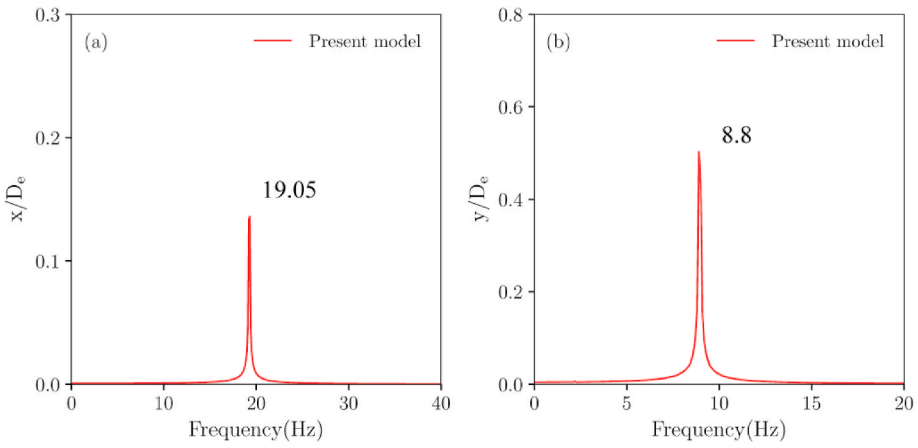

Fig. 11. The amplitude spectrum of the flexible riser without internal flow with $U_e = 1.6$m/s.
(a) The IL dominating frequency; (b) The CF dominating frequency.

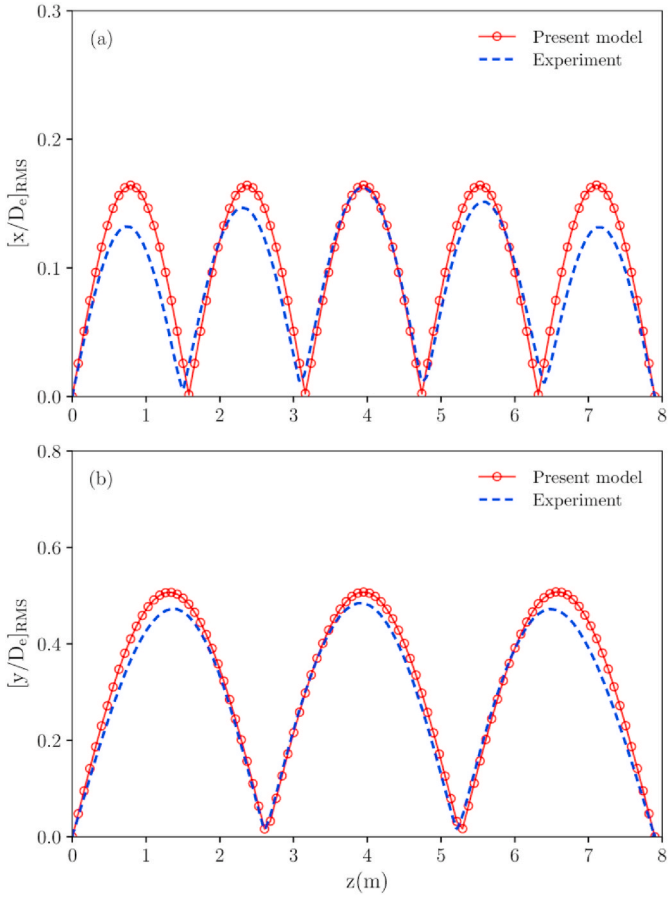

Fig. 12. The RMS displacements of the flexible riser without internal flow with $U_e = 1.6$m/s.
(a) The IL RMS displacement; (b) The CF RMS displacement.

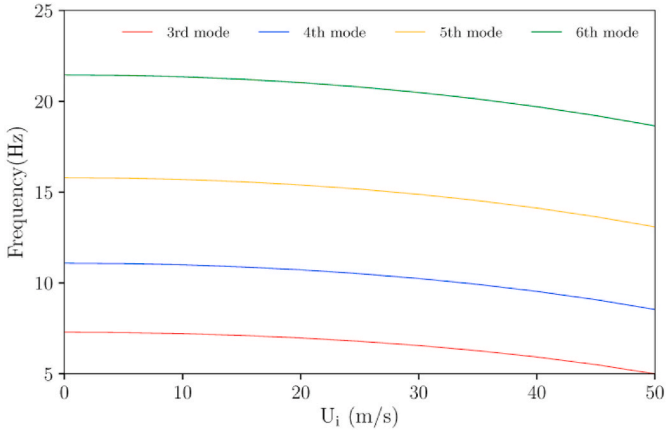

Fig. 13. The varying natural frequencies of the flexible riser with the increase of U_i.

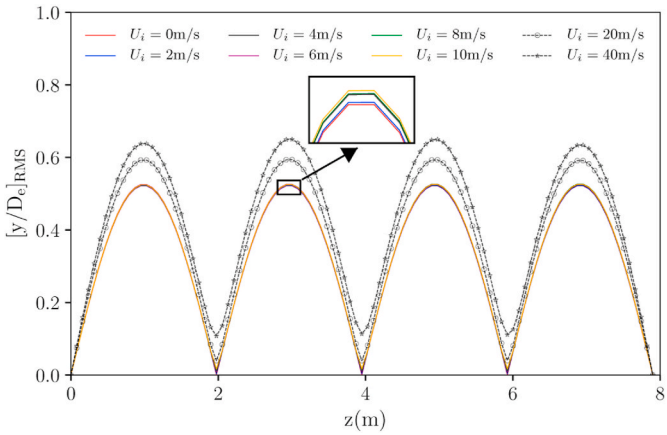

Fig. 14. Variation of the CF RMS displacement with the increase of U_i.

power accounts for the change of the IL RMS displacement. As a result, the consideration of the internal flow deceases the maximum IL RMS displacement.

It should be noted that the dominating mode of the flexible riser in IL direction changes from the 5th mode response to the 6th mode response when the internal flow velocity is increased up to 40 m/s (Fig. 15). This change can be also found in the work of Duan et al. (2018), where the mode transition is also observed for both IL and CF responses. The mode transition can be attributed to the change of the flexible riser stiffness with the increase of U_i. And it should be pointed out that the mode transition could occur when the internal flow velocity is large enough under the same external velocity. It should be also noted that no mode transition is detected for the CF VIV response of the flexible riser in this study, which implies that larger U_i is required for the occurrence of the mode transition in CF direction during our simulation.

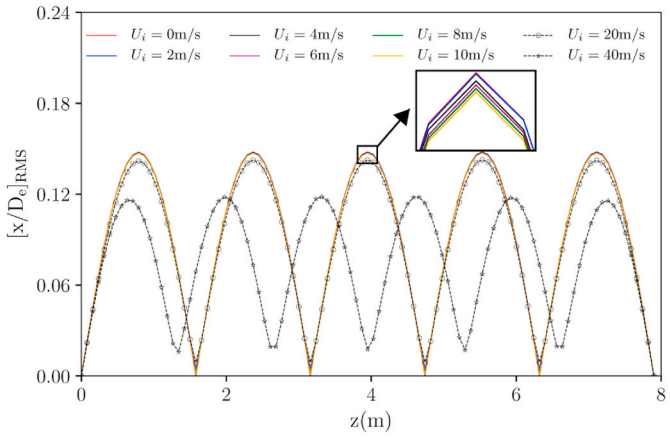

Fig. 15. Variation of the IL RMS displacement with the increase of U_i.

The trajectory of the flexible riser with $U_e = 1.6$m/s under different internal flow velocities is plotted in Fig. 16. It is clearly observed that the mean deflections in IL direction and the CF RMS displacement increase with the increase of the internal flow velocity. Furthermore, their maximum values are obtained when the internal flow velocity $U_i =$ 40m/s during our simulation. And the IL RMS displacement shows a decreasing trend here, with a minimum value at $U_i = 40$m/s, as shown in Figs. 15 and 16. It should be noted that the change of dominating mode in IL direction is also detected. And the flexible riser response is changed from the 5th mode response to the 6th mode response in IL direction when the internal flow velocity is increased up to 40 m/s. But no mode transition is observed in CF direction for the flexible riser here even when $U_i = 40$m/s.

3.2.2. IL and CF dominating frequencies

As for the dominating frequencies in IL and CF directions, the amplitude spectra of the flexible riser at nodes 37 and 50 with different U_i are demonstrated in Figs. 17 and 18. Obviously, both the IL and CF dominating frequencies decrease with the increase of the internal flow velocity when there appears no mode transition. And this decrease is particularly notable when the internal flow is increased largely. As shown in Figs. 17 and 18, the values of IL and CF dominating frequencies are reduced to 15.2 Hz and 10.5 Hz when $U_i = 20$m/s. The variation trend of the dominating frequency compares very well with the experimental observations in Guo and Lou (2008). The reason for the decrease of the IL and CF dominating frequencies is that the change of the natural frequency accounts for this phenomenon. As shown in Fig. 13, the natural frequencies of the flexible riser decrease with the increase of the internal flow velocity. When the specific excitation mode response is excited in IL and CF directions, the IL and CF excitation force frequencies are supposed to be locked onto these specific natural frequencies, causing the flexible riser to vibrate in accordance with these specific natural frequencies. Therefore, the IL and CF dominating frequencies decrease with the increase of U_i, in accordance with the changing trend of the natural frequencies of the flexible riser.

It should be emphasized that when the mode transition occurs, the VIV dominating frequencies change notably (Fig. 17). As shown in Fig. 17, when the internal flow velocity is increased up to 40 m/s, the dominating frequency in IL direction is changed to approximately 20.1 Hz. Such change can be attributed to that the VIV response is locked onto another natural frequency when the dominating modes change.

3.2.3. Drag coefficient

The drag coefficients based on Vandier's model is illustrated in Fig. 19. It is obvious that the internal flow velocity has an evident effect on the drag coefficients C_D. As shown in Fig. 19, the drag coefficient C_D is strongly related to the RMS displacement in CF direction (Eq. (6)) and shows a similar trend with the change of the CF RMS displacement. With the increase of the internal flow velocity, the maximum value of C_D is magnified under the same external flow velocity. The maximum value of C_D increases from approximately 2.4 at $U_i = 0$m/s to around 2.6 with $U_i = 40$m/s. This notable change of C_D can be attributed to the increase of the relative velocity between the flexible riser and the external flow. When the internal flow is considered, the CF RMS displacements are amplified while the RMS amplitudes in IL direction is decreased. Therefore, due to the change of RMS displacement and the almost stable vibration period, the velocity components in IL direction are enlarged, leading to the increase of the relative velocity between the flexible riser and the external flow. As a consequence, the drag forces in IL direction are magnified. Correspondingly, the drag coefficient C_D increases while the internal flow velocity is increased. As will be discussed, the magnification of the drag coefficient could also make a contribution to the increase of the IL mean deflection.

3.2.4. IL mean deflection

The IL mean deflection of the flexible riser with the increase of the internal flow velocity are examined here. The mean deflections in IL direction with different internal flow velocities are shown in Fig. 20. It can be seen that the largest deflection is always located at the midpoint of the flexible riser, regardless of the value of the internal flow velocity. While the internal flow velocity is increased, the IL mean deflection tend to be larger. For example, the maximum value of the IL mean deflection is approximately 3.9 with $U_i = 0$m/s. While U_i is increased to 40 m/s, the maximum value of the IL mean deflection can be up to about 8.2. One of the main reasons for this phenomenon is that the magnification of the drag coefficient of the flexible riser accounts for the increase of the IL mean deflection, which has been discussed in Section 3.2.3 (Fig. 19). When the internal flow is transported in the riser, the drag coefficient is enlarged due to the change of IL and CF displacements, thereby intensifying the riser mean deflection in IL direction with the increase of the internal flow velocity. Another potential factor leading to the increase of the IL mean deflection could be attributed to the centrifugal forces induced by the internal flow. When the internal flow begins to move in the riser, the centrifugal force is induced due to the transportation of the internal flow (Paidoussis (1987)). The occurrence of the centrifugal force could lead to the amplification of the IL mean deflection under the same external flow velocity, which is worthy of further exploration in the future.

3.3. VIV dynamics of a flexible riser with various internal flow densities

As the internal flow is an important factor to affect the VIV response in engineering, the VIV dynamics of a flexible riser considering internal flow with various densities are studied here. The density of the internal flow $\rho_i = 1000$kg/m^3, 2000 kg/m^3 and 3000 kg/m^3 is chosen here. The external and internal flow velocities are set to 1.6 m/s and 10 m/s respectively. And VIV dynamics of the flexible riser, such as the IL and CF RMS displacements and dominating frequencies as well as the drag coefficients, are mainly investigated and analyzed. Firstly, with the increase of the internal flow density, the variation of the dimensional natural frequencies is analyzed and plotted in Fig. 21. It can be observed that the increase of the internal flow density can decrease the natural frequencies of the flexible riser.

3.3.1. IL and CF RMS displacements and dominating modes

For the IL and CF RMS displacements, the trends of their changes with different internal flow densities are illustrated in Figs. 23 and 24. Clearly, the change of the internal flow density has an evident influence on the RMS displacement and dominating mode in both IL and CF directions. As shown in Figs. 23 and 24, with the increase of the internal flow density, the maximum IL RMS displacement decreases while the maximum CF RMS displacement shows an increasing trend. It can be found that the maximum IL RMS displacement is approximately 0.155

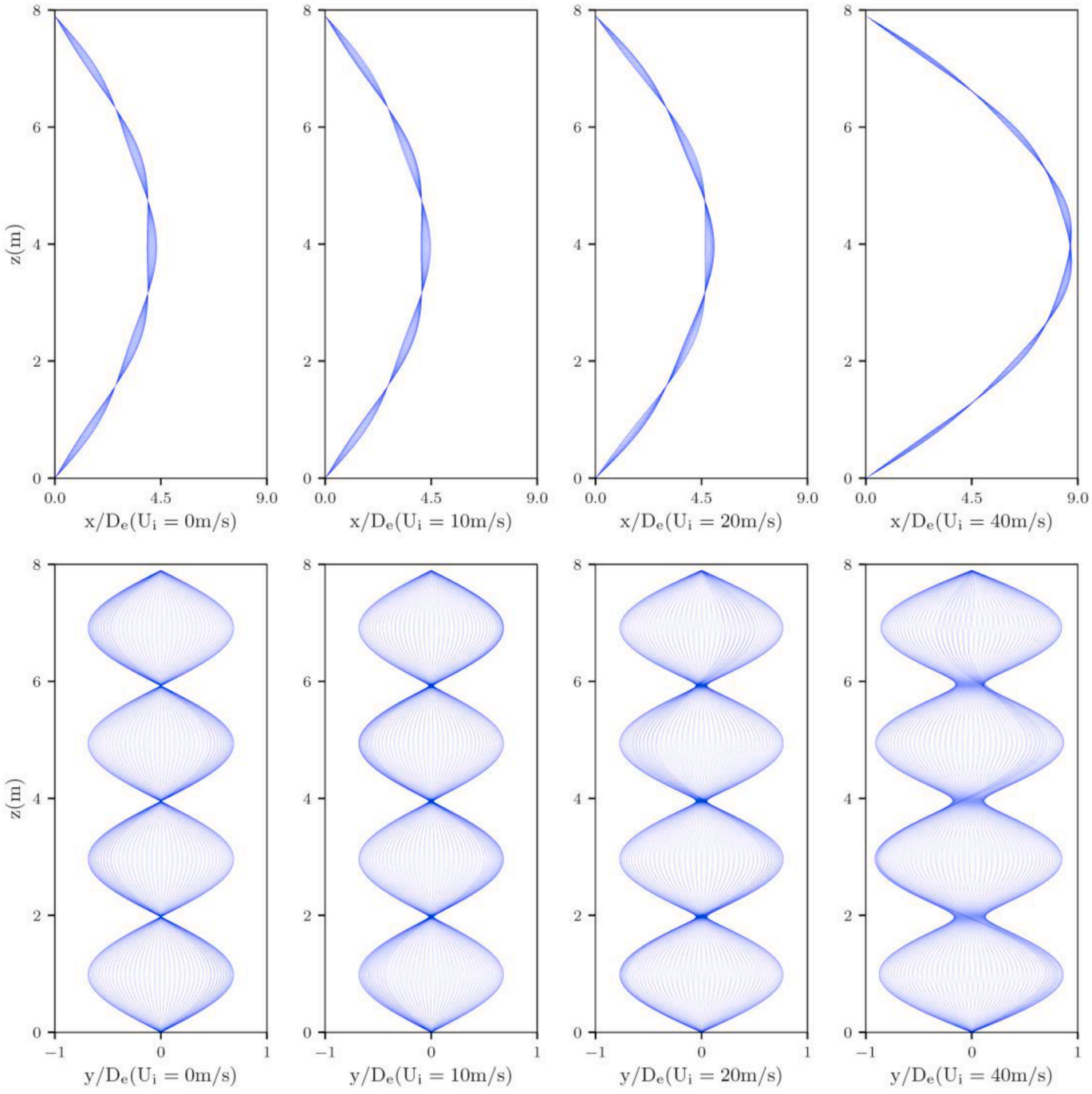

Fig. 16. The trajectory of the flexible riser with different internal flow velocities.

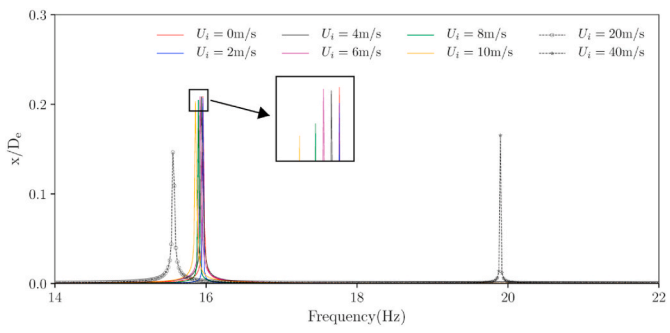

Fig. 17. Variation of the IL dominating frequency with the increase of U_i.

with $\rho_i = 1000\text{kg/m}^3$. When the density of the internal flow is up to 3000 kg/m^3, the maximum value of RMS displacement in IL direction decreases to around 0.14. As is discussed in the former subsection, the IL mean deflections contribute to the change of the IL RMS displacements. When the IL mean deflection increases, the IL RMS displacement tend to be decreased. Since larger IL mean deflection is observed for higher internal flow density, the RMS displacement in IL direction is reduced with the increase of ρ_i. In addition, another potential reason for the decrease of the IL RMS displacement is that less energy is responsible for the change of IL RMS displacement because more energy is allocated for the increase of the IL mean deflection and CF RMS displacement.

However, the changing trend of the CF RMS displacement is totally opposite to that of the IL RMS displacement. It can be seen from Figs. 22 and 23 that with the increase of the internal flow density, the CF RMS

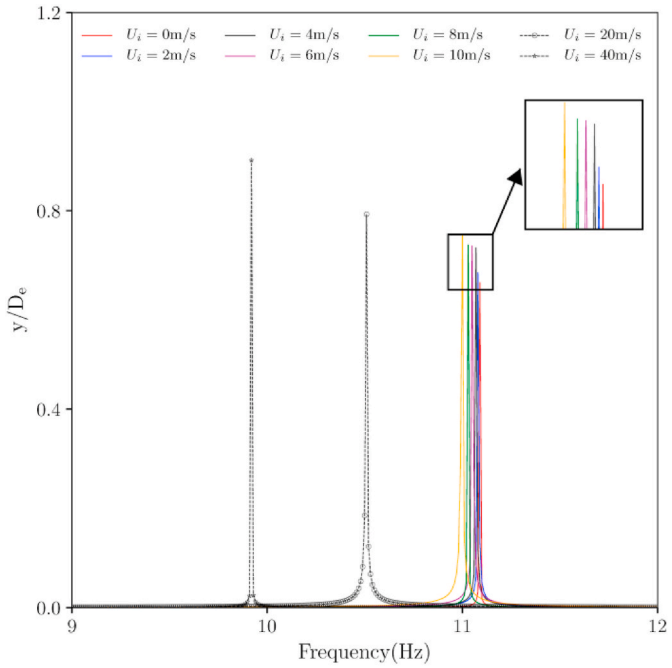

Fig. 18. Variation of the CF dominating frequency with the increase of U_i.

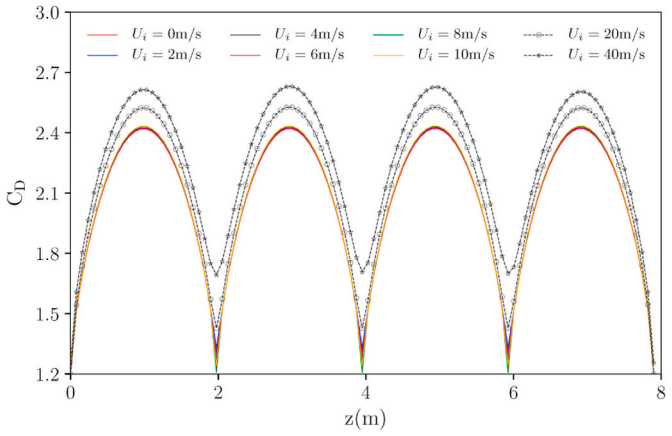

Fig. 19. Variation of the drag coefficient with the increase of U_i.

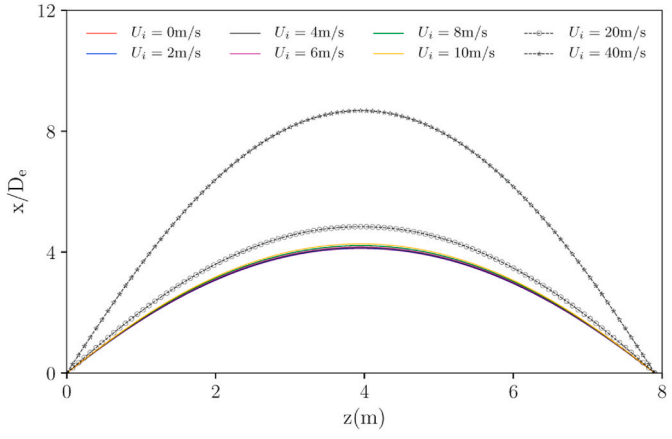

Fig. 20. Variation of IL mean deflection with the increase of U_i.

displacement is increased evidently. The maximum CF RMS

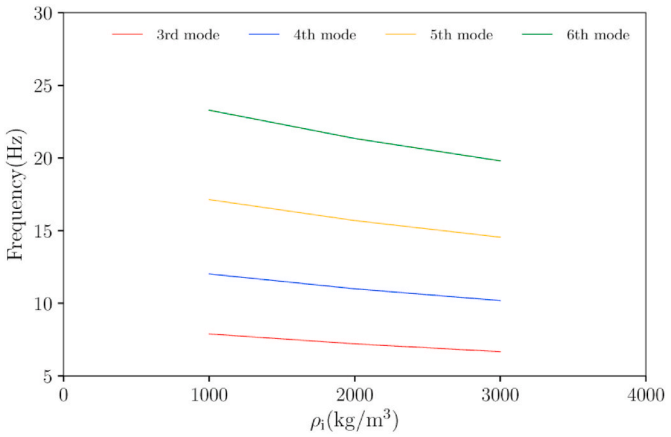

Fig. 21. The varying natural frequencies of the flexible riser with the increase of ρ_i.

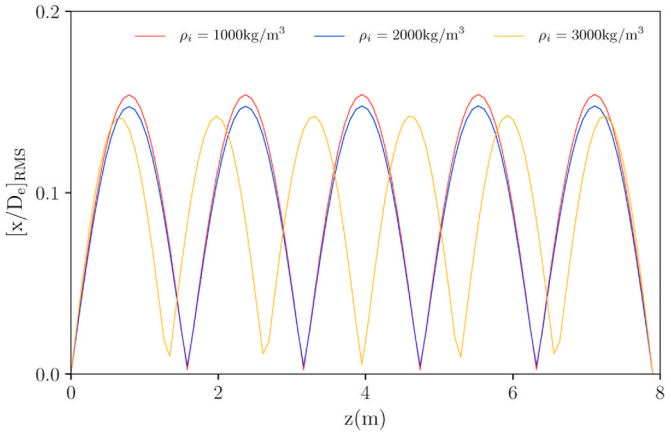

Fig. 22. Variation of the IL RMS displacement with the increase of ρ_i.

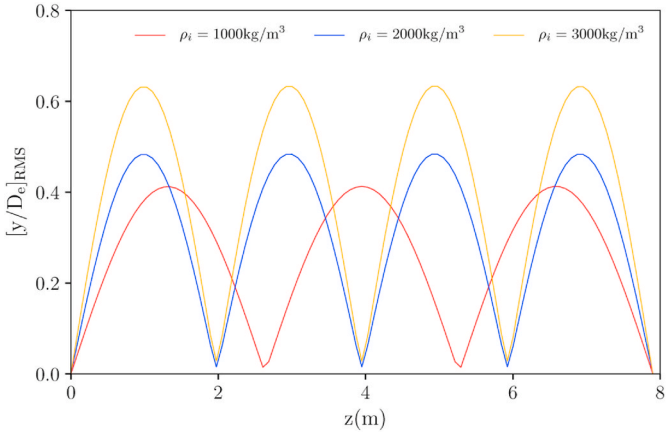

Fig. 23. Variation of the CF RMS displacement with the increase of ρ_i.

displacement is changed from 0.4 to 0.62 when internal flow density ρ_i increases from 1000 kg/m^3 to 3000 kg/m^3. The reason for this change is similar to that elaborated in Section 3.2.1. With the increase of the internal flow density, more energy flows into the structural system, leading to an oscillation with larger amplitudes in CF direction when the vibration of the riser achieves balance.

In addition, the dominating modes in IL and CF directions for the flexible riser are obviously affected by the change of the internal flow

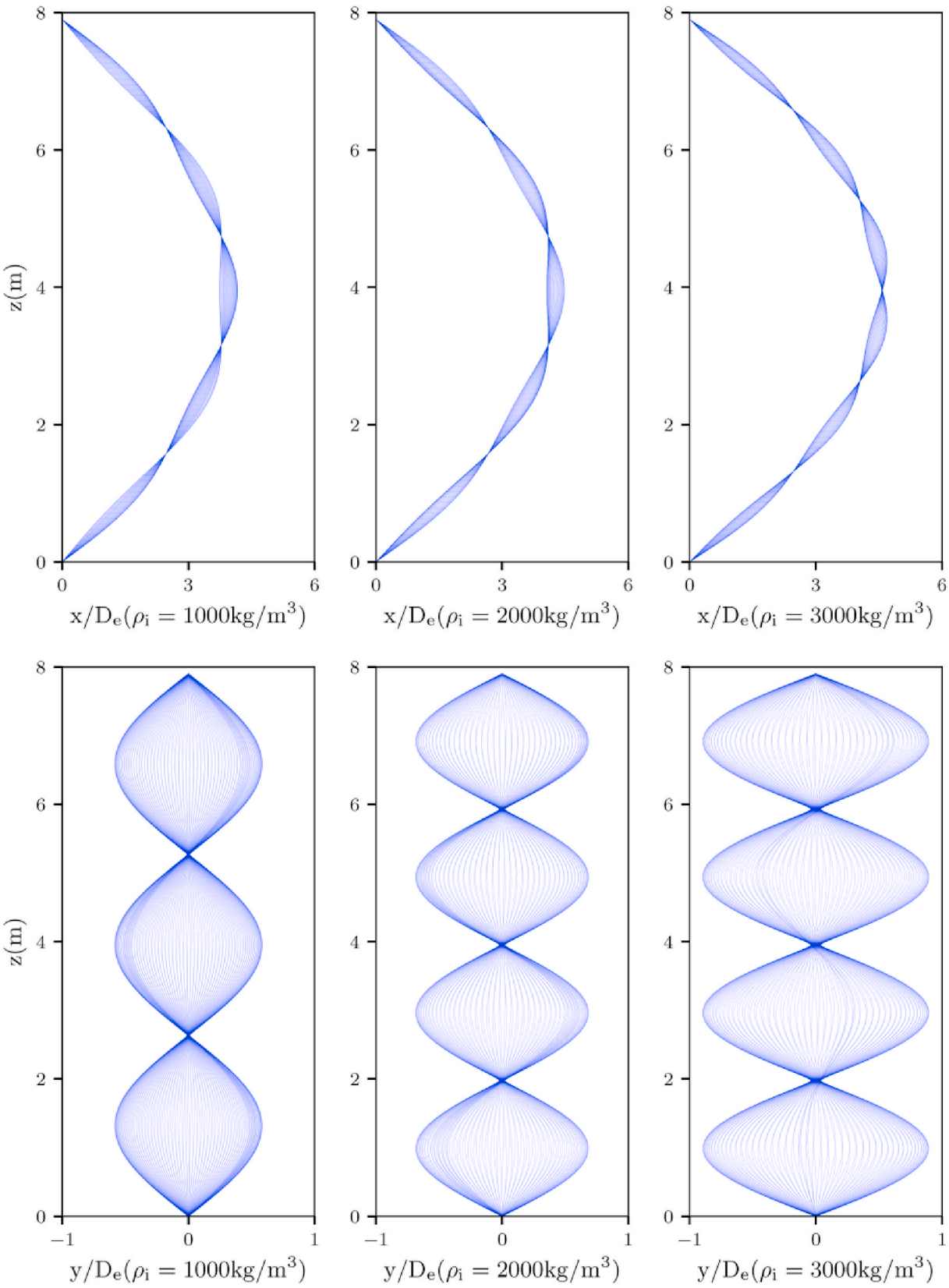

Fig. 24. The trajectory of the flexible riser with different internal flow densities.

density (Figs. 22–24). With the increase of the internal flow density ρ_i, both the IL and CF dominating modes are increased. When ρ_i is increased from 1000 kg/m^3 to 3000 kg/m^3, the IL dominating mode is changed from the 5th to 6th while the dominating mode in CF direction is increased from then 3rd to 4th. This evident mode transition can be attributed to the change of the riser stiffness, which indicates that the riser stiffness is susceptible to the change of the internal flow density.

3.3.2. IL and CF dominating frequencies

The variation of the IL and CF dominating frequencies is presented in Figs. 25 and 26. Similar to those in Section 3.2.2, the change of IL and CF dominating frequencies with different internal flow densities is closely related to the dominating modes in IL and CF directions, respectively. It can be observed from Figs. 25 and 26 that under different internal flow densities, the IL and CF dominating frequencies are also obviously influenced by the IL and CF dominating modes. Take the CF response as an example, the CF dominating frequency changes from 7.9 Hz to 11.0 Hz when the CF dominating mode is increased from the 3rd to 4th due to the increase of internal flow density. And similar change is also observed for the IL dominating frequency. This frequency transition is also because the response of the flexible riser is locked onto different natural frequencies due to the change of internal flow density, which is similar to the factor leading to the change of the dominating frequency when the internal flow velocity is increased. It should be emphasized that when the dominating mode is not changed with the increase of the internal flow density, the dominating frequencies in IL and CF directions decrease. As shown in Figs. 25 and 26, when ρ_i is increased from 1000 kg/m^3 to 3000 kg/m^3, the IL dominating frequency is reduced from 17.1 Hz to 15.8 Hz while the CF dominating frequency decreases from 11.0 Hz to 10.2 Hz. Such change can be also attributed to the decrease of the natural frequencies with the increase of the internal flow density.

3.3.3. Drag coefficient

The variation of the drag coefficient C_D with different internal flow densities is illustrated in Fig. 27. It can be found that with the increase of the internal flow density ρ_i, the maximum value of the drag coefficient C_D increases when the same dominating mode is excited with different internal flow densities. When ρ_i is increased from 1000 kg/m^3 to 3000 kg/m^3, the maximum drag coefficient is increased from approximately 2.4 to 2.65. This variation of C_D can be explained by the magnification of the relative velocity between the flexible riser and the external flow, which leads to the increase of the IL drag force. Besides, the drag coefficient is also related to the CF dominating mode under different internal flow densities.

3.3.4. IL mean deflection

The change of the IL mean deflection with the increase of ρ_i is demonstrated in Fig. 28. It can be easily found that the IL mean deflection of the flexible riser increases with the increase of the internal flow density. As is seen in Fig. 28, the maximum IL mean deflection is about 3.5 with ρ_i = 1000kg/m^3. Whereas its maximum value increases

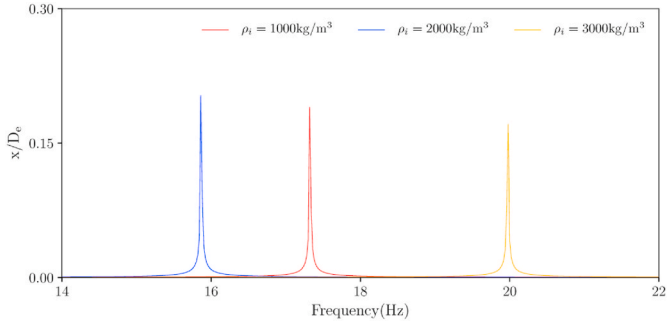

Fig. 25. Variation of the IL dominating frequency with the increase of ρ_i.

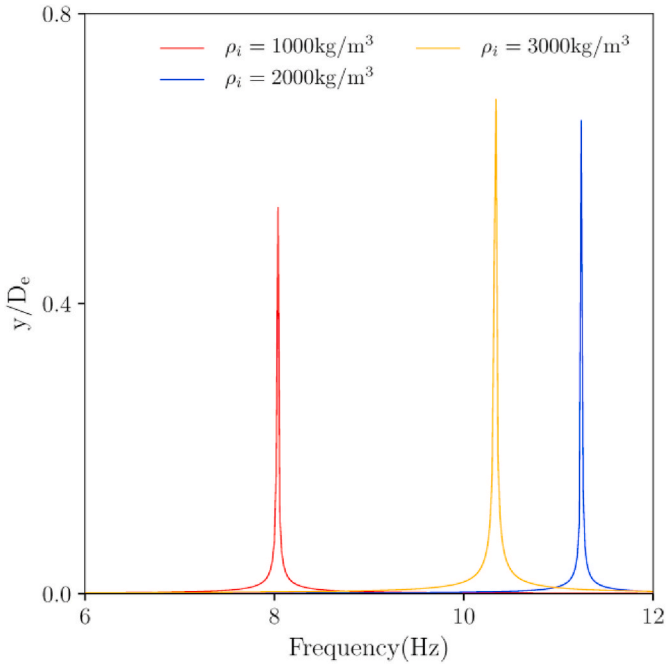

Fig. 26. Variation of the CF dominating frequency with the increase of ρ_i.

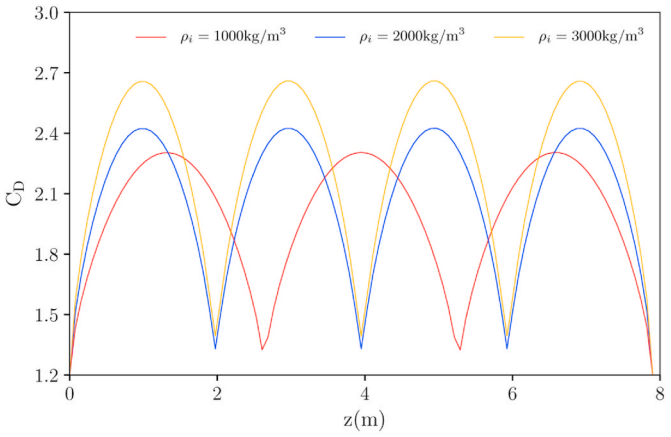

Fig. 27. Variation of the drag coefficient with the increase of ρ_i.

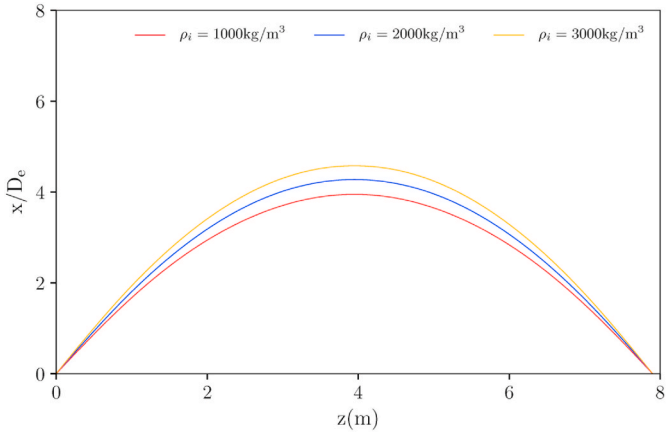

Fig. 28. Variation of the IL deflection with the increase of ρ_i.

up to approximately 4.5 when $\rho_i = 3000\text{kg/m}^3$. Similarly, the enlargement of the IL mean deflection due to the increase of the internal flow density shares the same reasons with that caused by the internal flow velocity increasing. One of the main reasons for such change is that with higher internal flow density ρ_i, the drag coefficient tends to be larger (Fig. 27), causing the flexible riser to deflect further in the IL direction from its equilibrium position. And the centrifugal force induced by the internal flow should also be considered as a potential factor which is responsible for the increase of the IL mean deflection.

3.4. VIV dynamics of a flexible fluid-conveying riser with different external flow velocities

As external flow has been proved to have an important effect on VIV dynamics, it is necessary to examine VIV responses of a flexible fluid-conveying riser with different external flow velocities. Since VIV dynamics of the flexible fluid-conveying riser shows a similar changing trend with different internal flow velocities and densities for all the external flow velocities, VIV responses with constant internal flow velocity and density are examined here while the external flow velocity is increased. Therefore, VIV dynamics of a flexible riser with internal flow density $\rho_i = 2000\text{kg/m}^3$ and internal flow velocity $U_i = 20\text{m/s}$ is studied here while the external flow velocity ranges from 0.4 m/s to 2.0 m/s ($U_e = 0.4\text{m/s}$, 0.8 m/s, 1.2 m/s, 1.6 m/s and 2.0 m/s).

3.4.1. IL and CF RMS displacements and dominating modes

As shown in Figs. 29 and 30, the IL and CF RMS displacements of the flexible fluid-conveying riser subjected to different external flow velocity U_e are demonstrated. It can be seen that under all the studied external flow velocities, the maximum IL RMS displacement of the flexible riser decreases and the maximum RMS displacement in CF direction shows an increasing trend when the internal flow is taken into consideration. As discussed in subsection 3.2.1, the increase of the maximum CF RMS displacement can be attributed to the power transferred into the riser system due the internal flow while the increase of the IL mean deflection is mainly responsible for the decease of the maximum IL RMS displacement. Note that the increase of U_e can have an effect on mode transition of the flexible fluid-conveying riser. As seen in Fig. 29, when there exists internal flow in the flexible riser, the mode response in IL direction changes from the 3rd and 4th mode responses to the 4th and 5th mode responses respectively while the external flow velocity is increased to 0.8 m/s and 1.2 m/s. These changes can be explained by that due to the increase of the external flow velocity, the vortex shedding frequency is increased. As a consequence, the frequency of the external hydrodynamic force is locked onto a higher natural frequency of the fluid-conveying riser, leading to the occurrence of mode transition.

3.4.2. IL and CF dominating frequencies

The IL and CF dominating frequencies of the flexible fluid-conveying riser under different external flow velocities U_e are illustrated in Figs. 31 and 32. Clearly, the dominating frequencies in both IL and CF directions are increased with the increase of the external flow velocity. It can be observed that with the increase of U_e, the IL dominating frequency increases from approximately 4.0 Hz to 21 Hz while the dominating frequency in CF direction is changed from about 2.0 Hz to 11 Hz. The reason for this phenomenon is that when the external flow velocity U_e is increased, the corresponding vortex shedding frequency is changed. Consequently, new mode response is excited as the external hydrodynamic force frequency is locked onto a new natural frequency of the flexible fluid-conveying riser.

It should be noticed that the IL and CF dominating frequencies are decreased under all external flow velocity while the internal flow is considered, except for the cases with the occurrence of mode transition ($U_e = 0.8\text{m/s}$ and 1.2 m/s). This can be attributed to the decrease of the natural frequency of the flexible riser due to the existence of the internal flow. But when mode transition occurs, new mode response is excited, causing that the flexible fluid-conveying riser vibrates with a new frequency, as shown in Fig. 31. Thus, frequency transition occurs for the IL VIV response when $U_e = 0.8\text{m/s}$ and 1.2 m/s.

3.4.3. Drag coefficient

The variation of the drag coefficient of the flexible fluid-conveying riser with different external flow velocities is shown in Fig. 33. It can be seen that the drag coefficient of the flexible fluid-conveying riser under all external flow velocities is increased while the internal flow is taken into account. Similar reason as that in subsection 3.2.3 and 3.3.3 is shared here. As the relative velocity between the flexible riser and the external flow is enlarged with the increase of the external flow velocity, the IL drag force is increased, causing the enlargement of drag coefficient. Besides, the drag coefficient is also related to the CF dominating mode under different external flow velocities.

3.4.4. IL mean deflection

Likewise, the IL mean deflection also shows an increasing trend under all external flow velocities while the flexible riser transports fluid

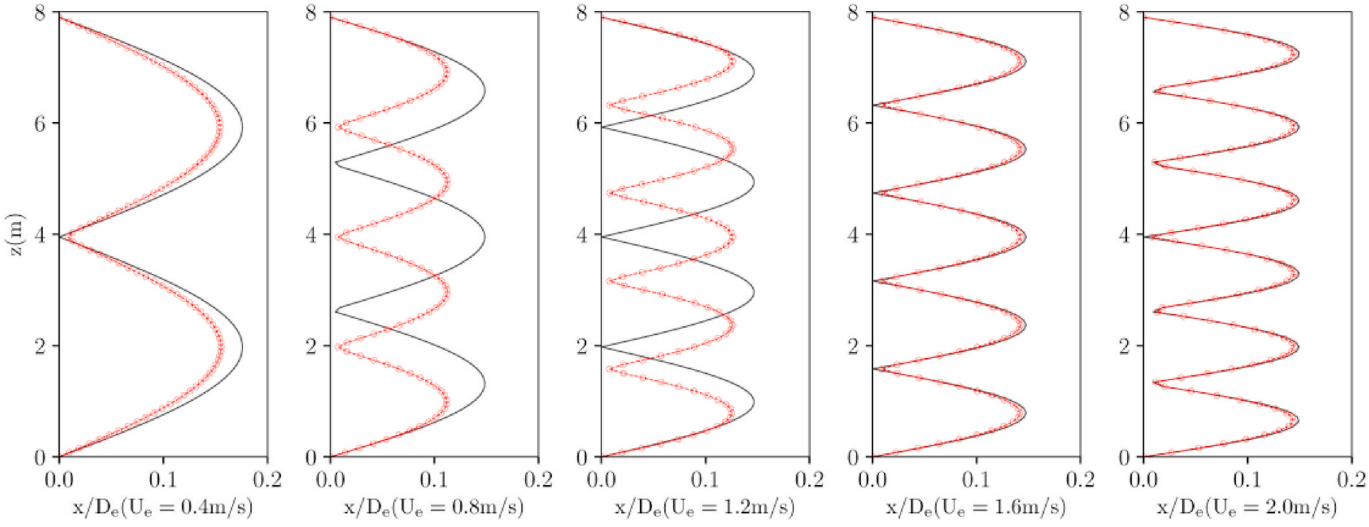

Fig. 29. Variation of the IL RMS displacement with the increase of U_e.
(Line: $U_i = 0\text{m/s}$; Dash line with circle: $U_i = 20\text{m/s}$).

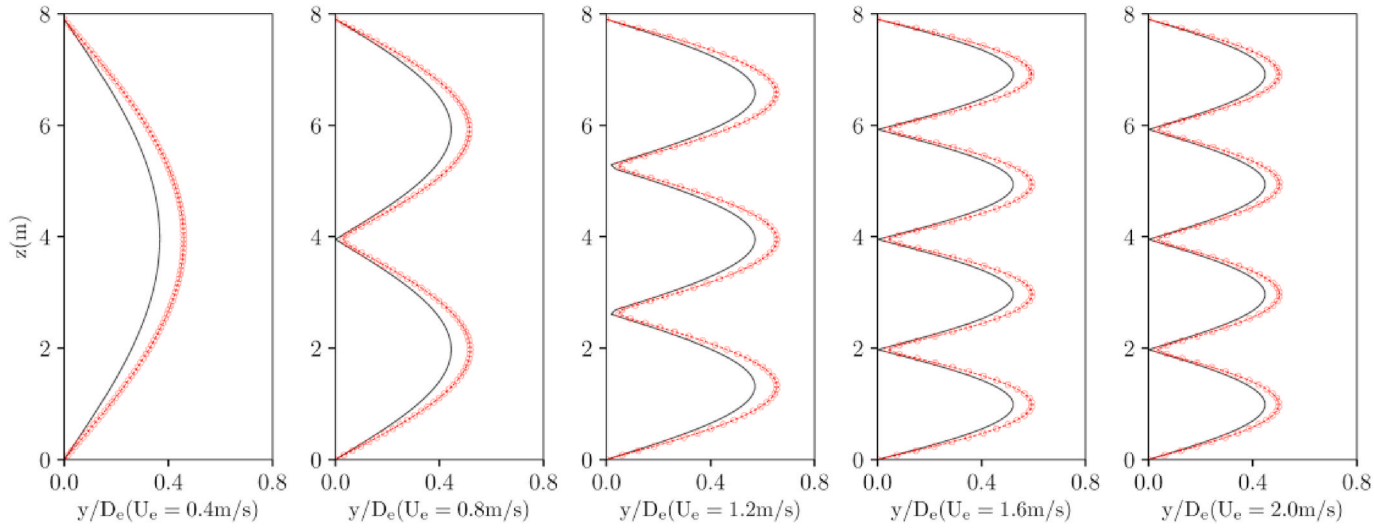

Fig. 30. Variation of the CF RMS displacement with the increase of U_e.
(Line: U_i = 0m/s; Dash line with circle: U_i = 20m/s).

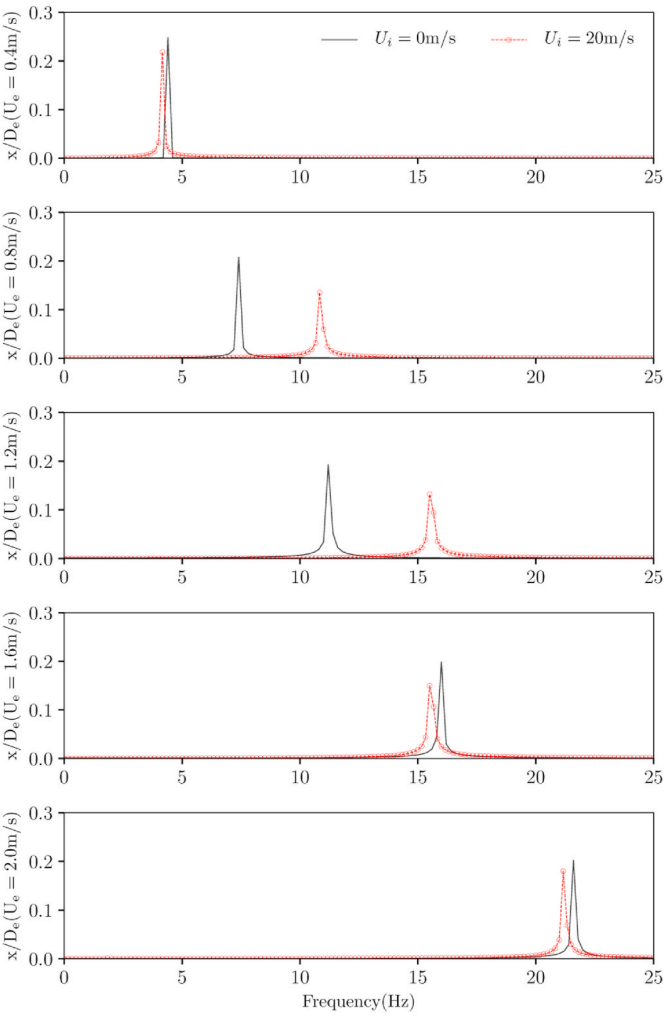

Fig. 31. Variation of the IL dominating frequency with the increase of U_e.

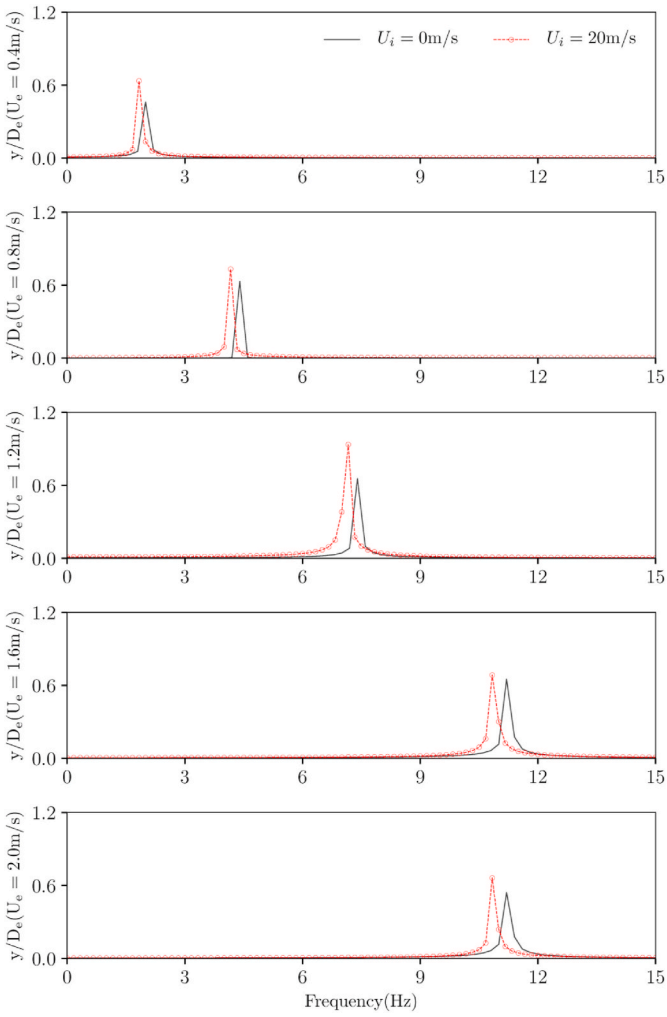

Fig. 32. Variation of the CF dominating frequency with the increase of U_e.

inside, as is plotted in Fig. 34. In addition, the IL mean deflection of the flexible fluid-conveying riser is increased with the increase of the external flow velocity. This is because the amplification of both the external flow velocity and drag coefficient accounts for the increase of the IL mean deflection while there exists fluid transporting in the flexible riser.

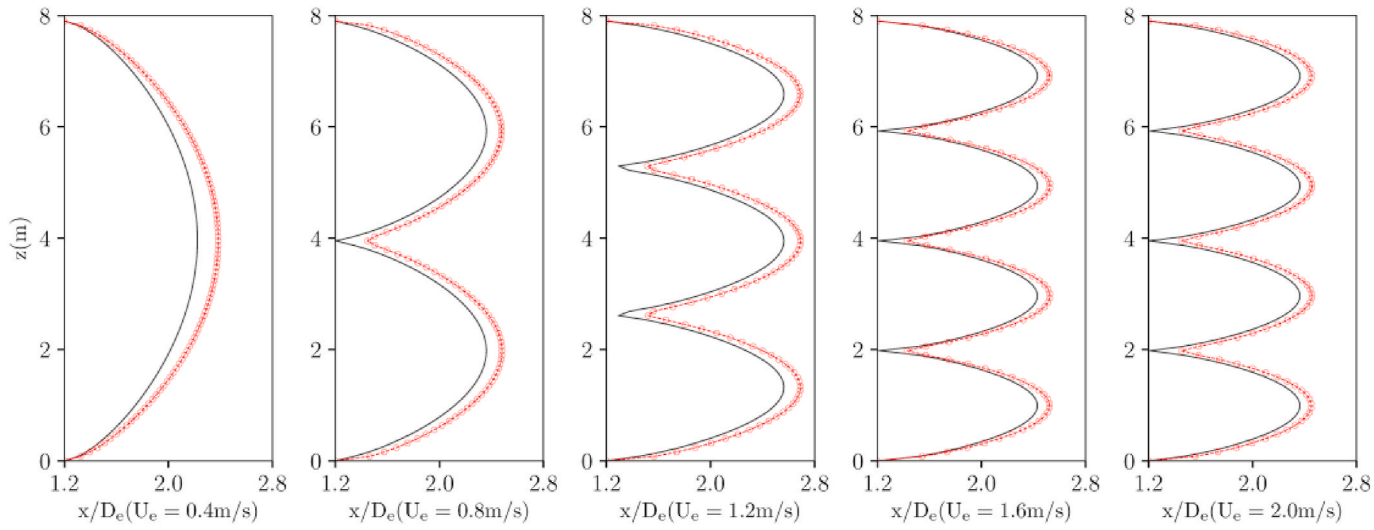

Fig. 33. Variation of the drag coefficient with the increase of U_e.
(Line: U_i = 0m/s; Dash line with circle: U_i = 20m/s).

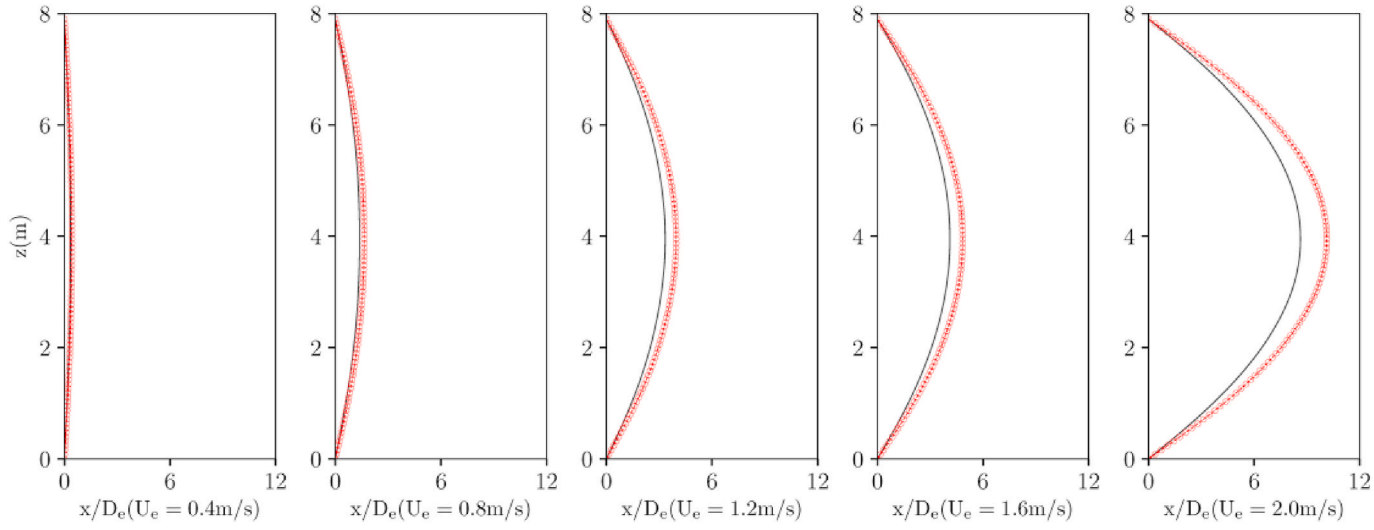

Fig. 34. Variation of the IL mean deflection with the increase of U_e.
(Line: U_i = 0m/s; Dash line with circle: U_i = 20m/s).

4. Conclusions

Based on the semi-empirical time domain prediction method proposed by Zhang et al. (2018), the three-dimensional VIV dynamics of a flexible riser transporting internal flow axially is examined in this paper. Correspondingly, main VIV characteristics, such as the RMS displacements, the dominating modes and frequencies in IL and CF directions as well as the IL mean deflection and the drag coefficient, are analyzed and discussed while the velocity and density of the internal flow are changed with various external flow velocities. During our simulation, the finite element method is utilized to discretize and solve the governing equations of the flexible riser numerically. Then the VIV response of the fluid-conveying flexible riser is demonstrated with various parameters of internal and external flows.

It is found that the increase of internal flow velocity and density can decrease the natural frequencies of the flexible riser, thereby causing the dominating modes in IL and CF directions to switch due to the excitation of new mode response under constant external flow velocity. Moreover, since more energy flows into the structural system with the increase of the internal flow velocity and density, the CF RMS displacement is magnified when the riser oscillation achieves balance. However, the RMS displacement in IL direction shows a decreasing trend due to the allocated power and IL mean deflection. As for the IL and CF dominating frequencies, both of them are reduced with the increase of the internal flow velocity and density when no mode transition occurs. It should be noted that there appears frequency transition in IL and CF direction if new mode response of the flexible riser is triggered. In addition, the drag coefficient is enlarged with the increase of the internal flow velocity and density due to the magnification of the relative velocity between the external flow and the flexible riser. Consequently, the IL mean deflection, which is determined by the enlarged drag coefficient, is amplified obviously with the increase of the internal flow velocity and density. Moreover, when the flexible fluid-conveying riser is subjected to different external flow velocities, VIV dynamics shows a similar changing trend with the increase of internal flow velocity and density.

The finding of this study can serve as a reference for the design and production in engineering. But there remains much work to be undertaken. Firstly, VIV dynamics of a flexible riser under various types of external flow should be researched, such as shear flow and oscillatory flow. The VIV response of the flexible riser can be much more

complicated while both the internal flow and complex external flow are taken into account. Besides, as the flexible riser is used for the transportation of the manganese nodules during deep ocean mining, the solid-liquid two-phase flow should be considered while the riser conveys internal flow. And scaled experiments should be carried out so that the mechanism and characteristics of VIV dynamics of the flexible riser with internal flow can be investigated and understood thoroughly.

CRediT authorship contribution statement

Jinlong Duan: Conceptualization, Methodology, Investigation, Software, Validation, Data curation, Visualization, Writing - original draft, Writing - review & editing. **Jifu Zhou:** Conceptualization, Methodology, Supervision, Visualization, Writing - review & editing. **Yunxiang You:** Conceptualization, Methodology. **Xu Wang:** Writing - review & editing.

Declaration of competing interest

The authors declare that they have no known competing financial interests or personal relationships that could have appeared to influence the work reported in this paper.

Acknowledgement

The authors acknowledge the supports of the National Key R&D Program of China (2017YFC1404200), National Natural Science Foundation of China (Grants 11572332) and the Strategic Priority Research Program of the Chinese Academy of Sciences (Grant XDB22040203, XDA22000000). Insightful advice from Dr. Yang Qu and Dr. Mengmeng Zhang at Shanghai Jiao Tong University is also gratefully acknowledged.

References

Ali, S.H., Giurco, D., Arndt, N., Nickless, E., Brown, G., Demetriades, A., Durrheim, R., Enriquez, M.A., Kinnaird, J., Littleboy, A., et al., 2017. Mineral supply for sustainable development requires resource governance. Nature 543 (7645), 367.
Atadan, A.S., Calisal, S.M., Modi, V.J., Guo, Y., 1997. Analytical and numerical analysis of the dynamics of a marine riser connected to a floating platform. Ocean Eng. 24 (2), 111–131.
Bearman, P.W., 2011. Circular cylinder wakes and vortex-induced vibrations. J. Fluid Struct. 27 (5–6), 648–658.
Bourguet, R., Karniadakis, G.E., Triantafyllou, M.S., 2011. Vortex-induced vibrations of a long flexible cylinder in shear flow. J. Fluid Mech. 677, 342–382.
Cabrera-Miranda, J.M., Paik, J.K., 2019. Two-phase flow induced vibrations in a marine riser conveying a fluid with rectangular pulse train mass. Ocean Eng. 174, 71–83.
Chaplin, J.R., King, R., 2018. Laboratory measurements of the vortex-induced vibrations of an untensioned catenary riser with high curvature. J. Fluid Struct. 79, 26–38.
Chatjigeorgiou, I.K., 2010. On the effect of internal flow on vibrating catenary risers in three dimensions. Eng. Struct. 32 (10), 3313–3329.
Dai, H.L., Wang, L., Qian, Q., Ni, Q., 2013. Vortex-induced vibrations of pipes conveying fluid in the subcritical and supercritical regimes. J. Fluid Struct. 39, 322–334.
Duan, J., Chen, K., You, Y., Li, J., 2018. Numerical investigation of vortex-induced vibration of a riser with internal flow. Appl. Ocean Res. 72, 110–121.
Gao, Y., Fu, S., Ren, T., Xiong, Y., Song, L., 2015. VIV response of a long flexible riser fitted with strakes in uniform and linearly sheared currents. Appl. Ocean Res. 52, 102–114.
Gopalkrishnan, R., 1993. Vortex-induced Forces on Oscillating Bluff Cylinders. Massachusetts Institute of Technology, Cambridge, MA, USA. Ph. D thesis.
Guo, H., Lou, M., 2008. Effect of internal flow on vortex-induced vibration of risers. J. Fluid Struct. 24 (4), 496–504.
Huera-Huarte, F.J., Bangash, Z.A., Gonzalez, L.M., 2014. Towing tank experiments on the vortex-induced vibrations of low mass ratio long flexible cylinders. J. Fluid Struct. 48, 81–92.
Jiang, T., Liu, Z., Dai, H., Wang, L., He, F., 2019. Nonplanar multi-modal vibrations of fluid-conveying risers under shear cross flows. Appl. Ocean Res. 88, 187–209.
Joshi, V., Jaiman, R.K., 2017. A variationally bounded scheme for delayed detached eddy simulation: application to vortex-induced vibration of offshore riser. Comput. Fluid 157, 84–111.
Joshi, V., Gurugubelli, P.S., Yenduri, A., Jaiman, R.K., Adaikalaraj, P.F.B., 2017. Investigation on standing and traveling wave response patterns in long flexible risers. In: ASME 2017 36th International Conference on Ocean, Offshore and Arctic Engineering. American Society of Mechanical Engineers Digital Collection (OMAE2017-61590).
Keber, M., Wiercigroch, M., 2008. Dynamics of a vertical riser with weak structural nonlinearity excited by wakes. J. Sound Vib. 315 (3), 685–699.
Knudsen, T.H., Sævik, S., Thorsen, M.J., 2016. Numerical analysis of combined VIV and slug flow in time domain. In: ASME 2016 35th International Conference on Ocean, Offshore and Arctic Engineering. American Society of Mechanical Engineers Digital Collection.
Lie, H., Larsen, C.M., Vandiver, J.K., 1997. Vortex induced vibrations of long marine risers; model test in a rotating rig. In: Proceedings from OMAE 1997, Yokohama, Japan.
Meng, D., Chen, L., 2012. Nonlinear free vibrations and vortex-induced vibrations of fluid-conveying steel catenary riser. Appl. Ocean Res. 34, 52–67.
Meng, S., Zhang, X., Che, C., Zhang, W., 2017. Cross-flow vortex-induced vibration of a flexible riser transporting an internal flow from subcritical to supercritical. Ocean Eng. 139, 74–84.
Ortega, A., Rivera, A., Nydal, O.J., Larsen, C.M., 2012. On the dynamic response of flexible risers caused by internal slug flow. In: ASME 2012 31st International Conference on Ocean, Offshore and Arctic Engineering. American Society of Mechanical Engineers Digital Collection, pp. 647–656.
Paidoussis, M.P., 1987. Flow-induced instabilities of cylindrical structures. Appl. Mech. Rev. 40, 163–175.
Païdoussis, M.P., 2014. Fluid-structure Interactions, Slender Structures and Axial Flow, second ed., vol. 1. Academic Press, California, USA.
Passano, E., Larsen, C.M., Lie, H., Wu, J., 2016. VIVANA—Theory Manual Version 4.8. Trondheim, Norway.
Qu, Y., Metrikine, A.V., 2020. A single van der pol wake oscillator model for coupled cross-flow and in-line vortex-induced vibrations. Ocean Eng. 196, 106732.
Sarpkaya, T., 1977. Transverse Oscillations of a Circular Cylinder in Uniform Flow, Part 1. Naval Postgraduate School, Monterey, CA, USA.
Sarpkaya, T., 2004. A critical review of the intrinsic nature of vortex-induced vibrations. J. Fluid Struct. 19 (4), 389–447.
Seyed-Aghazadeh, B., Edraki, M., Modarres-Sadeghi, Y., 2019. Effects of boundary conditions on vortex-induced vibration of a fully submerged flexible cylinder. Exp. Fluid 60 (3), 38.
Sharma, R., 2017. "Deep-sea Mining: Current Status and Future considerations." Deep-Sea Mining. Springer, Cham, pp. 3–21.
Song, L.J., 2016. Investigation on the Hydrodynamics of a Flexible Riser under Vortex-Induced Vibration. Shanghai Jiao Tong University, Shanghai, China. Ph. D thesis.
Song, J.N., Lu, L., Teng, B., Park, H.I., Tang, G.Q., Wu, H., 2011. Laboratory tests of vortex-induced vibrations of a long flexible riser pipe subjected to uniform flow. Ocean Eng. 38 (11–12), 1308–1322.
Song, L., Fu, S., Cao, J., Ma, L., Wu, J., 2016. An investigation into the hydrodynamics of a flexible riser undergoing vortex-induced vibration. J. Fluid Struct. 63, 325–350.
Soni, P.K., 2008. Hydrodynamic Coefficients for Vortex-Induced Vibrations of Flexible Beams. NTNU, Trondheim, Norway. Ph. D thesis.
Thorsen, M.J., Sævik, S., 2018. An analytical model of the effect of internal density waves in risers subjected to vortex shedding. In: The 28th International Ocean and Polar Engineering Conference. International Society of Offshore and Polar Engineers.
Thorsen, M.J., Sævik, S., Larsen, C.M., 2014. A simplified method for time domain simulation of cross-flow vortex-induced vibrations. J. Fluid Struct. 49, 135–148.
Thorsen, M.J., Challabotla, N.R., Sævik, S., Nydal, O.J., 2019. A numerical study on vortex-induced vibrations and the effect of slurry density variations on fatigue of ocean mining risers. Ocean Eng. 174, 1–13.
Trim, A.D., Braaten, H., Lie, H., Tognarelli, M.A., 2005. Experimental investigation of vortex-induced vibration of long marine risers. J. Fluid Struct. 21 (3), 335–361.
Vandiver, J.K., 1983a. Drag Coefficients of Long Flexible Cylinders. Offshore Technology Conference, Houston, Texas, USA. OTC Paper No. 4490.
Vandiver, J., 1993b. Dimensionless parameters important to the prediction of vortex-induced vibration of long, flexible cylinders in ocean currents. J. Fluid Struct. 7 (5), 423–455.
Vandiver, J.K., 2003. SHEAR7 User Guide 4.5. Department of Ocean Engineering, Massachusetts Institute of Technology, Cambridge, MA, USA.
Violette, R., Langre, E., de Szydlowski, J., 2010. A linear stability approach to vortex-induced vibrations and waves. J. Fluid Struct. 26 (3), 442–466.
Wang, E., Xiao, Q., 2016. Numerical simulation of vortex-induced vibration of a vertical riser in uniform and linearly sheared currents. Ocean Eng. 121, 492–515.
Wang, L., Jiang, T.L., Dai, H.L., Ni, Q., 2018. Three-dimensional vortex-induced vibrations of supported pipes conveying fluid based on wake oscillator models. J. Sound Vib. 422, 590–612.
Williamson, C.H.K., Govardhan, R., 2008. A brief review of recent results in vortex-induced vibrations. J. Wind Eng. Ind. Aerod. 96 (6–7), 713–735.
Xu, W., Ma, Y., Ji, C., Sun, C., 2018. Laboratory measurements of vortex-induced vibrations of a yawed flexible cylinder at different yaw angles. Ocean Eng. 154, 27–42.
Yang, W., Ai, Z., Zhang, X., Chang, X., Gou, R., 2018. Nonlinear dynamics of three-dimensional vortex-induced vibration prediction model for a flexible fluid-conveying pipe. Int. J. Mech. Sci. 138, 99–109.
Zhang, M., Fu, S., Ren, H., Li, R., Song, L., 2018. A time domain prediction method for vortex-induced vibrations of a flexible pipe with time-varying tension. In: ASME 2018 37th International Conference on Ocean, Offshore and Arctic Engineering. American Society of Mechanical Engineers Digital Collection.
Zhu, H., Gao, Y., Zhao, H., 2018. Experimental investigation on the flow-induced vibration of a free-hanging flexible riser by internal unstable hydrodynamic slug flow. Ocean Eng. 164, 488–507.